IPSE/alpha-1 adopts an IgE-binding crystallin fold

A Crystallin Fold in the Interleukin-4-inducing Principle of *Schistosoma mansoni* Eggs (IPSE/alpha-1) mediates IgE Binding for Antigen-independent Basophil Activation

N. Helge Meyer ^{1,2,#}, Hubert Mayerhofer³, Konstantinos Tripsianes^{1,2,§}, Silke Blindow⁴, Daniela Barths⁴, Astrid Mewes⁴, Thomas Weimar⁵, Thies Köhli⁵, Steffen Bade⁶, Tobias Madl^{1,2,&}, Andreas Frey⁶, Helmut Haas⁴, Jochen Mueller-Dieckmann³, Michael Sattler^{1,2}, Gabriele Schramm⁴

¹Institute of Structural Biology, Helmholtz Zentrum München, 85764 Neuherberg, Germany

²Munich Center for Integrated Protein Science (CIPSM) and Biomolecular NMR, Department Chemie,

Technische Universität München, 85747 Garching, Germany

³EMBL Hamburg Outstation c/o Desy, 22603 Hamburg, Germany

⁴Cellular Allergology, Research Center Borstel, 23845 Borstel, Germany

⁵Institute of Chemistry, University of Lübeck, 23562 Lübeck, Germany

⁶Mucosal Immunology & Diagnostics, Research Center Borstel, 23845 Borstel, Germany

*Current address: European Medical School, Department of General and Visceral Surgery,
Universität Oldenburg, 26131 Oldenburg, Germany

§Current address: CEITEC-Central European Institute of Technology, Masaryk University, Brno,
Czech Republic

&Institute of Molecular Biology & Biochemistry, Center of Molecular Medicine, Medical University of Graz, 8010 Graz, Austria

Running Title: IPSE/alpha-1 adopts an IgE-binding crystallin fold

To whom correspondence should be addressed: Gabriele Schramm, Cellular Allergology, Research Center Borstel, Parkallee 1-40, 23845 Borstel, Germany, Tel: +49(0)4537 1885610, E-mail: gschramm@fz-borstel.de

Michael Sattler, Institute of Structural Biology, Helmholtz Zentrum München, 85764 Neuherberg, Munich Center for Integrated Protein Science (CIPSM) and Biomolecular NMR, Department Chemie, Technische Universität München, Lichtenbergstr. 4, 85747 Garching, Germany, Tel: +49 (0)89 289-13418 Fax: -13210, E-mail: Sattler@helmholtz-muenchen.de

Jochen Müller-Dieckmann, EMBL Hamburg Outsation c/o Desy, 22603 Hamburg, Tel.: +49(0) 40 42816-660, E-mail: jochen.mueller-dieckmann@uni-hamburg.de

Keywords: nuclear magnetic resonance (NMR), crystal structure, Immunoglobulin E (IgE), Schistosoma mansoni, innate immunity, interleukin-4, IPSE/alpha-1, basophil, beta-gamma-crystallin

Background: The Interleukin-4-inducing principle from *Schistosoma mansoni* eggs (IPSE/alpha-1) triggers basophils to release interleukin-4 and interleukin-13 in an IgE-dependent but antigen-independent way.

Results: Structure analysis identified IPSE/alpha-1 as a new member of the $\beta\gamma$ -crystallin superfamily with a unique IgE-binding loop.

Conclusion: IPSE/alpha-1 activates basophils *via* IgE-binding crystallin folds.

Significance: Schistosomes use unique mechanisms to manipulate the host's immune response.

ABSTRACT

IPSE/alpha-1, the major secretory product of eggs from the parasitic worm Schistosoma mansoni, efficiently triggers basophils to release the immunomodulatory key cytokine interleukin-4. Activation by IPSE/alpha-1 requires the presence of IgE on the basophils, but the detailed molecular mechanism underlying activation is unknown. NMR and crystallographic analysis of IPSEΔNLS, a monomeric IPSE/alpha-1 mutant, revealed that IPSE/alpha-1 is a new member of the $\beta\gamma$ -crystallin superfamily. We demonstrate that this molecule is a general

immunoglobulin-binding factor with highest affinity for IgE. NMR binding studies of IPSEANLS with the 180-kDa molecule IgE identified a large positively charged binding surface that includes a flexible loop, which is unique to the IPSE/alpha-1 crystallin fold. Mutational analysis of amino acids in the binding interface showed that residues contributing to IgE binding are important for IgE-dependent activation of basophils. As IPSE/alpha-1 is unable to cross-link IgE, we propose that this molecule, by taking advantage of its unique IgE-binding crystallin fold, activates basophils by a novel, cross-linking-independent mechanism.

Schistosomes are parasitic worms causing a chronic disease with more than 200,000 deaths per year alone in sub-Saharan Africa (World Health Organization, Schistosomiasis Facts, 2012). During acute infection, schistosome eggs induce an inflammatory T helper type 2 (Th2) response characterized by high Immunoglobulin (Ig)E titers and eosinophilia (1). Subsequently, the Th2 response is down-regulated by antiinflammatory mechanisms to restrict host tissue damage (1). In this context, the cytokine interleukin (IL)-4 plays an important role, first as key inducer cytokine for a Th2 response (2) and second as key factor for limiting extensive inflammation. The absence of IL-4 signaling in S. mansoni-infected mice, which are unable to produce IL-4 (IL-4-/- mice) or to react to IL-4 (IL-4 receptor alpha-chain-/- mice), is associated with massive intestinal inflammation and rapid death (3, 4). Recent studies suggest that basophils are involved in anti-helminth immunity (5, 6). They have been shown to migrate to parasite-affected tissues, where they become fully activated and represent the major source of IL-4. However, the mechanisms by which the parasites activate basophils remained elusive.

Previously, we identified a homodimeric 35 kDa glycoprotein secreted from live *S. mansoni* eggs, which induces the release of IL-4 from human and murine basophils (7, 8). This protein was called IPSE ('IL-4-inducing principle from *S. mansoni* eggs') (7), but was subsequently renamed IPSE/alpha-1 (9) since it was found to be identical with the major excretory/secretory schistosome egg antigen alpha-1 described earlier (10). IPSE/alpha-1 has a unique sequence;

apart from a predicted putative Greek key motif there is no similarity to any other known protein, except to translated cDNA sequences from S. japonicum and translated genomic sequences from S. haematobium (11). IPSE/alpha-1 triggers the release of IL-4 from basophils of non-sensitized healthy human donors, and intravenous injection of IPSE/alpha-1 into mice leads to basophil-IL-4 release in the liver, which, apart from the gut, is the major site of egg deposition during S. mansoni infection (8). Basophil activation by IPSE/alpha-1 was found to depend on the presence of IgE on the surface of the basophils irrespective of the IgE's antigen specificity (7, 12). IgE-dependent, antigenindependent basophil activation is well known from multivalent lectins or B cell superantigens, which cross-link IgE via binding to its carbohydrate side chains or directly to its immunoglobulin backbone, respectively (13, 14). However, molecular details of the mechanism of action of IPSE/alpha-1 are not yet known.

Here, we report NMR- and crystallographic structures of IPSEANLS, a monomeric deletion mutant of IPSE/alpha-1. IPSEΔNLS lacks a stretch of 10 amino acids at the C-terminus comprising a putative nuclear localization sequence (NLS) (15) and Cys132, which mediates a disulfide bridge for dimer formation of the native molecule (16). The structure consists of two symmetrically arranged Greek key motifs and exhibits high structural similarity with members of the \(\beta \gamma\)-crystallin superfamily. Biochemical studies show that IPSE/alpha-1 is a general immunoglobulin-binding factor binding to all isotypes, but with highest affinity to IgE. NMR chemical shift analysis combined with functional assays suggest that IPSE/alpha-1 interacts with IgE via a large surface area that includes a loop comprising positively charged and aromatic amino acids, which are critical for IgE binding. In contrast to lectins and B cell superantigens, our data obtained with soluble or immobilized molecules suggest that IPSE/alpha-1 is not able to cross-link IgE. Thus, we propose that IPSE/alpha-1 activates basophils by a novel IgE-dependent, antigen-independent mechanism that does not involve cross-linking of IgE.

Experimental Procedures

Sample Preparation – Unlabeled IPSE/alpha-1 protein has been prepared as described elsewhere (17). For preparation of

uniformly ¹³C¹⁵N- and ¹⁵N-labeled samples, bacteria were grown in M9 supplemented with ¹³C-labeled glucose and/or ¹⁵NH₄Cl, respectively. For preparation of ²H/¹⁵N/¹³C-labeled IPSEΔNLS the same protocol was employed but using [U-2H13C]-labeled glucose and growing bacteria in 100% D₂O. Point mutations were introduced in pProExHTb-IPSEΔNLS and pProExHTb IPSE using the Ouick-Change site directed mutagenesis protocol (Invitrogen). The corresponding proteins contain two additional residues at the N-terminus from a tobacco etch virus (TEV) protease cleavage site, which was introduced by the expression vector.

NMR Spectroscopy was carried out on a Bruker Avance III 750 MHz spectrometer equipped with a TXI probehead, a Bruker Avance III 600 MHz spectrometer equipped with a cryogenic TCI probehead or on an Avance I 900 MHz spectrometer equipped with a cryogenic TXI probehead. Unless stated otherwise, all experiments were carried out on a 1 mM uniformly ¹³C/¹⁵N-labeled IPSEΔNLS at 298 K. Spectra were processed with NMRPipe (18) and analyzed with Sparky 3 (Goddard, T. Kneller, D. (http://www.cgl.ucsf.edu/home/sparky). For backbone and side chain assignment CBCA(CO)NH, (H)CCH-**CBCANH** and TOCSY (19) spectra were recorded (20). Distance information was obtained from ¹⁵Nand ¹³C-edited NOESY spectra with a mixing time of 70 ms. 15 N R_1 and R_2 relaxation rates and ${}^{1}H}-{}^{15}N$ heteronuclear NOE data measured at 750 MHz proton Larmor frequency and 298 K as described (21). Relaxation delays of 0.0216, 0.054, 0.27, 0.81, 1.08, 1.4 and 1.62 s were used to measure R1 and 0.0144, 0.0288, 0.0576, 0.0864, 0.115, 0.173, 0.173 were used to extract R2 rates. Errors were estimated from duplicate measurements of two delays and Monte Carlo simulation. Uncertainty of the ratio of R2/R1 relaxation rates was determined by error propagation. Residue-specific tumbling correlation times, τ_c were calculated as described elsewhere (21).

Structure Calculation was performed by automated NOE cross-peak assignment using the software CYANA 3.0 (22). Automatically assigned NOEs and completeness of the NOE cross peaks were inspected manually. Distance restraints from the CYANA calculation and TALOS+ (23) derived torsion angles were used

in a water refinement calculation (24) applying the RECOORD protocol (25). Ramachandran plot statistics after refinement are as follows: 91.1% of residues in most favored regions, 8.9% in additional allowed regions, 0% in generously allowed regions and 0% in disallowed regions. Quality of the NMR-derived structure ensemble was validated using the iCING web server (http://nmr.cmbi.ru.nl/icing/), as well as PROCHECK (26) and WHATCHECK (27). Molecular images were generated using Pymol (Delano Scientific, http://www.pymol.org).

NMR Titrations – Uniformly ²H/¹⁵N/¹³C-labeled IPSEΔNLS was stepwise added to 100 μM IgE (Dianova) at ratios of 0.5:1 and 1:1 (IPSEΔNLS:IgE) and chemical shifts were recorded using CRINEPT-HMQC spectra (28). A CRINEPT spectrum of 100 μM ²H/¹⁵N/¹³C-labeled IPSEΔNLS was recorded as a reference.

X-ray Structure Determination – IPSEΔNLS was solved by molecular replacement using Phaser as implemented in CCP4 6.1.131 with the modified NMR structure as a search model. Coordinates of IPSEANLS were refined using REFMAC 5.6.0119 alternating with rounds of manual model building using the program Coot. Initial crystallization trials were performed in 96 well sitting drop vapor diffusion plates at 20°C at a protein concentration of 14mg ml⁻¹ using commercially available screens. Two conditions yielded small crystals, which were optimized through a combination of OptiSalt screening (Qiagen) and customized grid screens resulting in well diffracting crystals, which appeared after at least one week. Crystals were flash frozen at 100 K in precipitant solution containing 15% glycerol. Diffraction data were collected at a wavelength of 0.9762 Å using an ADSC Q315R detector at ID29 at the ESRF. The data were indexed and integrated using DENZO and scaled with SCALEPACK (29). The crystals belong to the space group $P6_1$ with cell axes of a = b =54.4 Å, c = 56.1 Å and diffracted to a resolution of 1.71 Å with one molecule in the ASU. The structure was determined by molecular replacement with PHASER (30) using the IPSE NMR structure with all the loops trimmed as a search model. The structure was refined using Refmac (31) with isotropic B-factors and manual rebuilding of protein was done with COOT (32). For more details see Table 1. The final model has no outliers in the Ramachandran plot and 98.92% of all residues in the favored region. A final check of the stereochemical quality of the final model was carried out using the program MolProbity (33).

Computational Modeling of IPSEΔNLS/IgE Fab complex structure was performed using the ClusPro web server (34). The lowest energy structure of the IPSEΔNLS NMR structure ensemble and an IgE Fc structure from the protein database (PDB accession code 2WQR) were used for the rigid body docking. Unstructured terminal residues were removed from the IPSEΔNLS structure. Attractive restrains were introduced for residues which were significantly broadened or experienced chemical shift perturbations in the NMR titration. Repulsive restraints were used for unaffected residues.

Size Exclusion Chromatography – IPSE/alpha-1 dimer was mixed with IgE or IgG in a 1:1 molar ratio, pre-incubated for 30 min at room temperature, and applied to a Superdex 200 10/300 GL column (GE Healthcare). Chromatography was performed in PBS, pH 7.4 at 0.4 ml/min at the ÄKTA-Purifier 10 (GE Healthcare). Fractions of 0.5 ml were collected and analyzed by SDS-PAGE and silver staining.

Surface Plasmon Resonance - Experiments were performed on a Biacore 3000 (GE Healthcare) and repeated at least twice. IgE or IgG were immobilized on a CM5 chip by standard amine coupling chemistry IPSE/alpha-1 dimer: IgE: 969 RU; IgG: 4435 RU; for IPSEANLS monomer: IgE: 5058 RU; IgG: 8428 RU). One flow cell was activated and deactivated without ligand for control purposes. Unspecific binding to the control flow cell was subtracted from the binding to the ligand-loaded flow cells. Running buffer was PBS, pH7.5. Regeneration was performed with 0.075% SDS in PBS, pH 7.5. Measurements were performed under the following conditions: Immobilized IgE: 100 - 700 nM IPSE/alpha-1 dimer with a flow rate of 10 µl/min for 10 min at 25°C, or 62.5 – 8000 nM IPSEANLS monomer with a flow rate of 10 µl/min for 10 min at 25°C. Immobilized IgG: 150 - 700 nM IPSE/alpha-1dimer with a flow rate of 5 µl/min for 20 min at 25°C or 125 -16,000 nM IPSEΔNLS monomer with a flow rate of 10 µl/min for 10 min at 25°C.

SDS-PAGE and Western Blotting were performed according to standard protocols as described previously (7). Materials were obtained from the following suppliers: human

IgG (Octagam); human IgE and human IgG Fab and Fc (Acris); human IgA (Dianova); human (Medac). Immunoglobulins **IgM** immunoglobulin fragments were detected by alkaline phosphatase (AP) - labeled antibodies (diluted between 1:10,000 and 1:40,000): goat anti-human IgE, goat anti-human IgG (Fc), goat anti-human IgA, goat anti-human IgM, and goat anti-human Ig (k light chain) (Dianova). Binding of IPSE/alpha-1 was detected by a monoclonal anti-IPSE/alpha-1 antibody 74-4B-7 followed by AP-goat anti-mouse IgG (Dianova) or using biotinylated IPSE/alpha-1 and subsequent incubation with AP-labeled streptavidin (SAV-AP) (Dianova). Dot blotting was performed using the SCR 96 D Minifold II-Dot Blotter (Schleicher & Schuell).

Sandwich Dot Blot was performed by dotting different amounts of human IgE (Acris) (4 – 0.5 pmol) onto nitrocellulose membrane. Following blocking of free binding sites, the membrane was incubated overnight either with IPSE/alpha-1 (125 pmol/ml), with anti-IgE (30 pmol/ml; positive control) or with buffer (negative control). Following a washing step, membranes were incubated with biotinylated IgE (500 ng/ml) for 2 h and, subsequently, with alkaline phosphatase-labeled streptavidin diluted 1:10,000 for 1 h.

For *Biotinylation*, 6 mg IPSE/alpha-1 in PBS, pH 8.5 was mixed with 1 ml of a freshly prepared solution of N-hydroxysuccinimidebiotin (Sigma-Aldrich) in DMSO (1 mg/ml) and incubated for 4 h at room temperature followed by dialysis against PBS pH 7.4. Biotinylated IPSE/alpha-1 was stored at -80°C.

Peptide Scan – Overlapping 15mer peptides were synthesized on cellulose membrane supports via the SPOT-technique according to Röckendorf et al. (35). After side chain deprotection of the peptides the membrane was incubated for 10 min with 15 ml of 100% (v/v) ethanol and subsequently washed three times, for 10 min each time, with 15 ml of phosphate buffered saline, pH 7.0 (PBS; 2.7 mM KCl, 1.5 mM KH₂PO₄, 136 mM NaCl, 8.1 mM Na₂HPO₄). For fake stripping, the membrane was incubated in an ultrasonic device twice, for 5 min each time, in 15 ml of N,N'-dimethylformamide, then for 5 min in 100 ml double-distilled water, then twice, for 7 min each time, in 15 ml of denaturing buffer (8 M urea, 1% (w/v) sodium dodecylsulfate, 0.5 % (v/v) \(\beta\)-mercaptoethanol x HOAc, pH 7.0) and finally three times, for 5 min

each time, in PBS. The membrane was then blocked for 4 h with 25 ml of 1% (w/v) casein (Hammarsten grade, BDH) in PBST (PBS containing 0.05% (v/v) Tween20). After a wash for 10 min with 20 ml PBS, the membrane was incubated over night in tight fitting trays at 4°C with 14.5 ml (2 ml/cm² membrane) of 6.7-8.3 nMol/ml IgE (Acris) that had been labeled according the manufacturer's instructions with DY781-N-hydroxysuccinimidylester (IgE-DY781: Dyomics) in blocking buffer. Subsequently, the membrane was washed five times, for 10 min each time, with 25 ml PBST and then for 10 min with 25 ml PBS. Fluorescence was quantitated and normalized to the mean fluorescence (=100%) of the parental peptide IPSE62-76 (Fig. 6D, inset: spots D1 and D2) (Odyssey Infrared Imager, Odyssey Software (v.1.2); Li-COR Biosciences).

Deglycosylation of Human IgG Fc Fragment by PNGase F Treatment - IgG Fc (Acris) was dialyzed against PBS, pH 7.5 containing 0.05 mM EDTA. 330 pmol IgG Fc were incubated with 5,000 mU PNGase F (Roche) in 100 mM sodium phosphate buffer containing 25 mM EDTA, pH 8.0, for 17 h at 37 °C. For control purposes IgG Fc was incubated with buffer alone. SDS-PAGE and Western blotting was performed as described above. Carbohydrates were detected by AP-labeled Aleuria aurantia agglutinin (AAA; 0.1 $\mu g/ml;$ Vector Laboratories).

Double **Immunodiffusion** Assay (Ouchterlony) – The immunodiffusion assay was performed according to standard procedures. 1% agarose (HEEO ultra quality, Roth) in barbitone buffer, pH 8.2 (0.04 M 5,5-diethylbarbituric acid sodium salt, 0.017 M 5,5-diethylbarbituric acid, both Merck, conserved with 0.015% (w/v) merthiolate, Sigma) was pipetted onto carrier film (agarose gel support film; FMC. Using a gel punching device (CAMAG), holes were punched into the gel and each was filled with 8 µl solution of binding partners (positions and concentrations see legend of Fig. 10D). After 48 h incubation the gels were pressed between two glass plates and several layers of pre-wetted filter paper with weights of 1 kg and 5 kg, respectively, for 10 min each. Gels were washed with 0.9% NaCl and distilled water and dried at 40°C before staining with Coomassie.

Induction of IL-4 Release from Human Basophils – Basophils were purified from peripheral blood of healthy human donors to a

mean purity of 99% (36). Purified basophils were cultured and stimulated as previously described (7). Incubation was performed in 100 ul of culture medium (Iscove's modified Dulbecco's medium supplemented with 100 U/ml penicillin G, 50 µg/ml transferrin, 5 µg/ml insulin, 100 µg/ml streptomycin and 10% fetal calf serum (PAA)) at a concentration of 10⁶ basophils /ml. Cells were stimulated in the presence of IL-3 (2.5 ng/ml) as a basophil survival factor with various stimuli at the concentrations indicated, and supernatants were collected after 18h and stored at - 20°C until further investigation. Interleukin-4 release was measured in the culture supernatants by using a two-site sandwich ELISA (Eli-Pair, Diaclone) according to the manufacturer's protocol.

Accession Codes – The atomic coordinates for the NMR ensembles and the crystal structures of IPSEΔNLS have been deposited in the Protein Data Bank under accession numbers 4AKA and 4EL6, respectively. The chemical shift assignments have been deposited in the Biological Magnetic Resonance Data Bank under accession number 17405.

Results

Solution Crystal and Structure IPSE/alpha-1 - IPSE/alpha-1 has recently been identified to be the major excretory/secretory component of S. mansoni eggs (37). However, apart from a translated cDNA sequence from S. japonicum (Acc. No. FN317557) and recently sequenced genes from S. haematobium predicted to encode excretory/secretory proteins (11), a BLAST search in the sequence database did not reveal any similar sequences. On the primary structure level, a Y/FXXXXY/FXG motif followed by a serine approximately 30 residues downstream suggested the presence of a Greek key motif. Premature full-length IPSE/alpha-1 consists of 134 amino acids including an Nterminal signal peptide (residues 1-20), which is cleaved upon release of the mature IPSE/alpha-1 (residues 21-134). In the following, the residue numbering refers to the position in premature full-length IPSE/alpha-1. For this study, we cloned and expressed mature IPSE/alpha-1 (residues 21-134) and a monomeric deletion mutant of IPSE/alpha-1, IPSEΔNLS (residues 21-124) which lacks 10 amino acids at the Cterminus including a positively charged NLS (15) 125-131) (residues and Cys132 responsible for dimer formation (Fig. 1A).

Expression in E. coli of both, wild-type IPSE/alpha-1 dimers and IPSEΔNLS monomers resulted in formation of inclusion bodies, which were solubilized by 8 M urea and refolded with physiological buffers containing the glutathione system GSH-GSSG to dimerization. Two N-glycosylation sites present on the natural IPSE/alpha-1 were found to be not involved in basophil activation. E. colinon-glycosylated IPSE/alpha-1 expressed exhibited the same functional activity as the glycosylated natural protein. Although neither the dimer nor the monomer expressed in E. coli were glycosylated, the wild-type IPSE/alpha-1 dimers aggregated after refolding concentrations above 0.2 mg/ml. In contrast, the IPSEΔNLS monomers remained highly soluble at concentrations >10 mg/ml and were thus suitable for structural studies (Fig. 1B).

To elucidate the molecular basis for the function of IPSE/alpha-1, we performed structural analysis of IPSEΔNLS using NMR spectroscopy and X-ray crystallography. NMR secondary chemical shift analysis indicated an all- β -strand secondary structure of IPSE Δ NLS (Fig. 1C). ¹⁵N NMR relaxation data showed that the polypeptide chain is rigid except for one loop (residues 62-69) which exhibits increased conformational flexibility (Fig. 1D). The tumbling correlation time $\tau_c \approx 7 \text{ ns}$ estimated from 15 N R_2/R_1 relaxation rates indicates that IPSEΔNLS (MW: 12 kDa) is a monomer in solution. This is in line with earlier studies demonstrating that the C-terminal cysteine (Cys132) absent in IPSEΔNLS is required for covalent dimerization of wild-type IPSE/alpha-1 (16). The ${}^{13}C^{\beta}$ secondary chemical shifts of six other cysteines in IPSEΔNLS reflect an oxidized state of the attached sulfur atoms, consistent with the presence of three intramolecular disulfide bridges.

The solution structure of IPSEΔNLS (**Fig. 2A, left**), was determined based on a large number of NOE-derived distance restraints and dihedral angle restraints derived from TALOS+(23) (**Table 1**). NOE patterns and chemical shifts indicated the presence of disulfide bonds between cysteines 23 and 26, 59 and 93 as well as 111 and 121, which served as additional restraints in the structure calculation.

Crystals of IPSEANLS, which diffracted to a resolution of 1.71 Å were obtained as described earlier (17). The crystallographic structure (**Fig.**

2A, right, Table 1) exhibited unambiguous electron density for the three disulfide bridges indicated above, whereas residues 64 to 68 within the flexible loop (see above) were not visible in the crystal structure due to missing electron density. The crystal and the NMR structure of IPSEANLS were in excellent agreement and superimposed with a backbone coordinate root mean square deviation (RMSD) of 0.5 Å. The structure of IPSEΔNLS consists of a sandwich of two β-sheets comprising eight anti-parallel β -strands (β 1- β 8), which form two Greek key motifs arranged in a pseudo 2-fold symmetry (Fig. 2B). The loops between the first two β -strands of each motif ($\beta 1/\beta 2$ and $\beta 4/\beta 5$, respectively) represent a characteristic β hairpin motif. The two β -sheets are formed by three strands of one Greek key motif each and a fourth β-strand contributed from the other Greek key, as is typically observed in crystallin folds (Fig. **2D**).

IPSE/alpha-1 Adopts a Crystallin Fold superfamily The βy-crystallin comprises structural proteins from the vertebrate eye lens and a few distant relatives found in lower eukaryotes and prokaryotes. Most of the eye lens proteins contain four Greek key motifs arranged in two domains. The structures of the C-terminal domain of human eye lens y-B-crystallin (PDB Acc. No. 2JDF), which is the best characterized member of the βy-crystallin superfamily (Fig. 3A, right) and IPSEΔNLS monomer (Fig. 3A, **left**), superimposed with a backbone coordinate RMSD of 1.7 Å Despite this strong structural similarity at the primary sequence level the conservation of IPSE and the C- or N-terminal domain of human eye lens γ-B-crystallin was less than 15% identity (Fig. 3C). Structural similarity in spite of low sequence identity has also been reported for several other members of the $\beta\gamma$ -crystallin superfamily in lower organisms (38). Another example, Spherulin 3A from Physarum polycephalum, which contains only one domain with two Greek key motifs dimerizes via a disulfide bridge near the Nterminus to restore the two-domain crystallin fold. IPSE/alpha-1 was found to dimerize in a similar fashion although the respective cysteines are located at the C- rather than at the Nterminus (Fig. 3B). Irrespective of the overall low sequence similarity, the highly conserved signature sequence Y/FXXXXY/FXG represents a hallmark of the crystallin fold. The aromatic residues in this motif interact with a conserved serine on the third beta strand of each Greek key motif (corresponding to β 3 and to β 7 of Greek key motifs 1 and 2, respectively). Interestingly, in Greek key motif 1 of IPSE/alpha-1 the spacing between the two tyrosine residues in the signature YDETYERG is shortened by one residue compared to other crystallin sequences (**Fig. 3C**). As a result, the tyrosine rings cannot stack with each other so that Tyr34 is solvent-exposed. However, the formation of the hairpin loop is not significantly affected (**Fig. 2D**).

Whilst the fold of the human lens γ-Bcrystallin is maintained by strong hydrophobic interactions in the protein core, the IPSE fold is stabilized by three disulfide bonds (23/26, 59/93 and 111/121) (Fig. 2B and C), consistent with its high stability over a wide pH range and against 2 M Urea. These disulfide bonds may compensate the lack of a tyrosine corner (39), which is present in most γ -crystallins (see γ -Bcrystallin, Tyr151 in Fig. 3A, right). A typical feature of a tyrosine corner is a hydrogen-bond between the hydroxyl-group of the tyrosine side chain (Tyr151 in Fig. 3A, right), and the peptide backbone two to five amino acids upstream stabilizing the formation of a β-hairpin. In contrast, the IPSE/alpha-1 fold and stability appears to depend on disulfide bridge formation, consistent with the observation that IPSEΔNLS rapidly precipitated under reducing conditions. Distinct from other proteins of the crystallin family, the β7 and the β4 strands of Greek key motif 2 in IPSE/alpha-1 are elongated (Fig. 3C). Furthermore, orthogonal stacking of Tyr74 and Tyr72 and additional hydrophobic contacts lead to a curvature of this β -sheet (**Fig. 3A, left**). The long flexible loop between the two Greek key motifs (residues 62-69; Fig. 3A and C, colored in green) turned out to be a unique feature of IPSE/alpha-1 compared to other crystallins.

IPSE/alpha-1 is an Immunoglobulin Binding Factor — Earlier, we demonstrated that the presence of IgE on the surface of basophils is essential for functional activity of IPSE/alpha-1. This prompted us to investigate the interaction of IPSE/alpha-1 with IgE, other immunoglobulin isotypes and further serum components. All experiments described in the following were performed with the IPSE/alpha-1 dimer, which is the basophil-activating form. Western blots from whole human serum samples demonstrated that IPSE/alpha-1 binds to the immunoglobulin

bands and to a band identified by N-terminal sequencing as transferrin (Tf), but not to other serum components (Fig. 4A). More detailed analysis confirmed that it binds to all human serum immunoglobulin isotypes (IgE, IgG, IgA, and IgM) in a non-antigen-specific manner (Fig. Thus, IPSE/alpha-1 is a general immunoglobulin-binding factor. Titration of IgE and IgG on dot blots suggested that IPSE/alpha-1 binds with higher affinity to IgE than to IgG (Fig. 4C). This finding was corroborated by size exclusion chromatography (SEC) of preformed IPSE/alpha-1-IgE and IPSE/alpha-1-IgG complexes in solution. IPSE/alpha-1-IgG, in IPSE/alpha-1-IgE, contrast to completely dissociated upon the mechanical shear forces during SEC. This demonstrated that IPSE/alpha-1 binds with considerably lower affinity to IgG than to IgE (Fig. 5).

In order to quantify the binding affinity of IPSE/alpha-1 to IgE and IgG, we performed surface plasmon resonance (SPR) assays with IPSE/alpha-1 dimer and IPSEΔNLS monomer. SPR assay with the IPSE/alpha-1 dimer (Fig. **6A**) showed that IPSE/alpha-1 clearly bind to immobilized immunoglobulins on the CM-5 sensor chip. However, the binding isotherms obtained upon analysis of the data showed a sigmoidal curve indicating a complex binding scenario of dimeric IPSE/alpha-1 to the dimeric immunoglobulins. As a consequence, simple curve fitting using the Langmuir (1:1) calculation was not applicable to determine quantitative affinity data. Thus, we performed additional SPR experiments with the monomeric mutant IPSEANLS (Fig.6B). Fitting of the binding isotherms using a 1:1 binding model revealed a K_D of 1.7 μM for the binding of IPSEΔNLS to IgE and 7.4 μM for the binding to IgG, which corresponds to a 4-fold higher binding affinity to IgE compared to IgG. This corroborates the earlier observations that IPSE/alpha-1 binds with higher affinity to IgE than to IgG, although one should keep in mind that the overall binding affinity of the dimer to IgE might differ from that of the monomeric mutant.

Analysis of the Interaction Sites of IPSE/alpha-1 with IgE – In order to map the binding interface of IPSE/alpha-1 with the IgE antibody, we compared NMR chemical shifts of IPSE Δ NLS free and IPSE Δ NLS bound to IgE at

molar ratios of 0.5:1 and 1:1 (IPSEΔNLS:IgE). Given the high molecular weight of the complex (≈ 200 kDa) 2 H-labeling of IPSE Δ NLS was required for sufficient sensitivity. Uniformly ²H/¹⁵N/¹³C-labeled IPSEΔNLS was titrated with unlabeled human IgE to monitor chemical shift perturbations (CSP) using ¹H, ¹⁵N correlation experiments. Upon binding of IPSEΔNLS to the 180 kDa IgE molecule, IPSEΔNLS signals experience extensive line broadening, that likely results from the low molecular tumbling rate and thus strongly increased NMR line widths in the high molecular weight complex. We therefore used relaxation optimized NMR experiments (28) to detect IPSEΔNLS bound to IgE (Fig. 7A). A number of amide proton signals close to the interaction site remain broadened beyond detection, while for several other signals significant chemical shift differences observed compared to free IPSEΔNLS. The binding kinetics of the IPSE/IgE interaction is slow at the NMR chemical shift time scale consistent with a low micromolar to nanomolar dissociation constant. The observed CSPs identify a large binding surface on one side of IPSEΔNLS that includes the flexible loop (residues 62-69) connecting the two Greek key motifs (Fig. 7A-C). The opposite side of the structure (\beta 1 and \beta 2 with the hairpin loop in Greek key motif 1, and β 7 and β 8 in Greek key motif 2 is largely unaffected by IPSE-binding to IgE. The amide group of Val63, which is in close proximity to the solvent exposed aromatic side chain of Phe62 in the flexible loop, experiences chemical the strongest perturbation. Another patch of strongly affected residues, e.g. Gly83, is in close spatial proximity to the highly conserved Tyr81. The NMR data thus indicated that the binding interface involves these aromatic side chains. Most of the interface is located in overall positively charged regions of the protein, especially the flexible loop (residues 62-69) and beta strand β 4. This implies an essential role of electrostatic and charged interactions.

Peptide scan analysis of the sequence requirements in the peptide comprising residues 62 to 76 revealed that exchanges of positively charged amino acids to either alanine or glutamate lead to a drastic decrease in IgE binding (B1, B2, B4 and D3, D4, D5, respectively) (**Fig. 7D**). This highlights the importance of the positive charges for the

IPSE/IgE interaction. In addition, exchange of the aromatic residues Tyr72 and 74, Trp73, Phe76, and Leu75 by alanines (C1, C2, C3, C4, C5) strongly decreases the binding affinity to IgE, demonstrating the importance of additional interactions. hydrophobic Interestingly, scrambling of the amino acid sequence did not change the binding intensity significantly, suggesting that the overall charge hydrophobicity might be even more important than the sequence itself. Taken together, the peptide scan and NMR titration, demonstrated the importance of positively charged and aromatic amino acid side chains for enabling effective binding of IPSE/alpha-1 to IgE.

The residues relevant for the interaction of IPSE/alpha-1 with IgE as determined by NMR and peptide scan experiments were further investigated by mutational analysis (Fig. 8). Mutations were introduced both into IPSEANLS (monomeric due to lack of the inter-chain disulfide bond) and into wild-type IPSE/alpha-1 (dimeric). The monomeric IPSEANLS mutants were analyzed by NMR for structural integrity (Fig. 9A, B); the dimeric IPSE/alpha-1 mutants were analyzed for immunoglobulin-binding (Western blotting; Fig. 8A) and for basophil IL-4-releasing capacity (Fig. 8B).

The mutants I108E/K109E, Q28R/E41K and D31K/E32K showed reduced immunoglobulin binding and loss of functional activity due to compromised *in vitro* folding. NMR analysis revealed that the monomeric IPSEANLS mutant I108E/K109E is unfolded in solution (**Fig. 9A**). In contrast, the monomeric mutants Q28R/E41K and D31K/E32K appeared folded in the NMR analysis. However, Western blot analysis of the corresponding dimeric mutant preparations revealed a shift in the dimer/monomer ratio towards the monomer (**Fig. 8A**). Thus, the reduced functional activity of these two preparations is potentially due to a reduced proportion of functionally active dimer.

All other IPSE/alpha-1 mutants were structurally intact as assessed by **NMR** (monomeric IPSEΔNLS mutants) and by monitoring the intensity of dimeric IPSE/alpha-1 bands on Western blots. The mutants K67E/R68E N80A/T82A and displayed immunoglobulin-binding and IL-4-inducing capacities similar to the wild-type IPSE/alpha-1. This is consistent with the fact that the respective residues are located outside (N80, T82) or at the edge (K67, R68) of the binding interface as assessed by NMR (Fig. 9C). The double mutant F62A/N64A exhibited reduced binding to IgG and IgE compared to the wildtype and markedly reduced basophil-activating capacity. The pronounced effect of the amino acid exchange in positions 62 and 64 corroborates the critical role of the flexible loop (aa 62-69) as the core of the immunoglobulin interaction site. The mutant T92Y/R127L is identical with a factor from S. mansoni eggs termed SmCKBP (40). SmCKBP has been reported to bind to, and neutralize, chemokines but to be unable to activate basophils. In accordance with this previous recombinant T92Y/R127L displayed markedly reduced immunoglobulin binding together with a complete lack of IL-4-releasing capacity. These results were consistent with the position of T92 within the binding surface as mapped by the NMR titrations (Fig. 8, 9C). Taken together, the mutational analysis showed a good correlation between the ability of IPSE/alpha-1 to bind immunoglobulins and to activate basophils. Our results suggest that IgE binding involves a binding surface which includes the unique flexible loop of the IPSE/alpha-1 crystallin fold, while functional activity requires the presence of dimeric IPSE/alpha-1.

IPSE/alpha-1 does not Cross-link IgE – The finding that only dimeric – but not monomeric – IPSE/alpha-1 is able to activate basophils suggests that the functional activity of this molecule involves cross-linking of receptorbound IgE, the classical mechanism seen with allergens, lectins and B cell superantigens. Since an antigen-specific binding mode (such as exhibited by an allergen) could be excluded, we asked whether IPSE/alpha-1 interacts with the carbohydrate side chains (like a lectin) or with the Fab or Fc regions of immunoglobulins (like a B cell superantigen). We therefore performed Western blot experiments with Fab and Fc fragments of human IgG. IgG was used as a paradigmatic immunoglobulin, as this isotype is available in large quantities and is bound by IPSE/alpha-1.

A lectin-like-binding of IPSE/alpha-1 to immunoglobulin glycan side chains could be excluded by comparing its binding to native (i.e. glycosylated) and to PNGase F-deglycosylated Fc fragments of IgG (Fab fragments of IgG are not glycosylated). Deglycosylation of IgG Fc was confirmed by Western blot analysis, as

deglycosylated IgG Fc was found to band at lower molecular weight than native IgG Fc (**Fig. 10A**). Moreover, the lectin *Aleuria aurantia* agglutinin that binds to fucose residues on native IgG no longer detected deglycosylated IgG Fc. In contrast, IPSE/alpha-1 recognized both, glycosylated and deglycosylated IgG Fc. This clearly rules out a lectin-like interaction between IPSE/alpha-1 and IgG, a finding which quite likely applies also to the other immunoglobulin isotypes (due to the highly conserved immunoglobulin domains).

To investigate whether IPSE/alpha-1 binds to the Fab or the Fc part of IgG, whole IgG and Fab and Fc fragments were analyzed for binding of IPSE/alpha-1 by Western blotting. IPSE/alpha-1 was found to bind to both, Fab and Fc fragments (**Fig. 10B**).

Typically, IgE-dependent activation basophils occurs via cross-linking of IgE on their surface as described for allergens, anti-IgE antibodies, lectins or B cell superantigens. Thus, expected the same mechanism for IPSE/alpha-1. However, methods to demonstrate cross-linking, such as sandwich dot blots and double immunodiffusion assay, showed, that IPSE/alpha-1 was not able to cross-link IgE. By sandwich dot blots we investigated, whether IPSE/alpha-1 cross-linked unlabeled membranebound IgE with labeled soluble IgE. While the blot with anti-IgE (positive control) showed a clear positive signal, the blot with IPSE/alpha-1 signal did not exceed background (buffer control) level indicating that IPSE/alpha-1 was not able to cross-link IgE (Fig. 10C). A background signal observed with ≥3.3 pMol IgE/dot likely resulted from the tendency of IgE to form aggregates at high concentrations. Analogous results were obtained with the double immunodiffusion assay. Binding partners were applied in different concentration ratios to wells punched in the agarose on microscope slides. After diffusion into the gel for 48 h, immunoprecipitation due to cross-linking of the binding partners was visualized by Coomassie staining. As expected, all ligand combinations used as positive controls (IgE/anti-IgE, IgG/anti-IgG, IgG/protein L (a B cell superantigen from Peptostreptococcus magnus) and IPSE/alpha-1/anti-IPSE antiserum) yielded clearly visible precipitin lines; but neither IPSE/IgE nor IPSE/IgG formed complexes large enough to precipitate in the gel, suggesting that IPSE/alpha-1 did not cross-link IgE or IgG in

solution (**Fig. 10D**). Of note, the small IPSE/alpha-1-IgE complexes formed at equivalence as assessed by size exclusion chromatography indicated a binding stoichiometry of one IPSE/alpha-1 dimer to one IgE molecule and, thus, confirmed that cross-linking did not take place (**Fig. 5**).

Discussion

evidence Accumulating suggests an important role of basophils for the immune response against helminth infection. However, the molecular mechanism of parasite-induced basophil activation is unknown for the majority of worm infections. In case of schistosomiasis, IPSE/alpha-1 represents the active principle responsible for activation of basophils (7). To better understand the molecular mechanisms by which IPSE/alpha-1 induces basophil IL-4 release from non-sensitized healthy individuals, we determined the structure of this molecule and investigated its interaction with IgE.

The solution and crystal structures of the monomeric IPSE Δ NLS classified IPSE/alpha-1 as a novel member of the $\beta\gamma$ -crystallin superfamily. $\beta\gamma$ -crystallins, such as the eye lens γ -B-crystallins, are characterized by extremely high stability towards harsh conditions such as extreme pH (pH 1), high temperature (70°C) and chaotropic agents (6 M urea) (38). For IPSE/alpha-1 such a stable structure might be important, since following secretion from schistosome eggs it has to withstand the aggressive environment of the inflammatory egg granuloma characterized by low pH and high levels of oxidative and other denaturing agents.

The structural and mutational analysis of the complex of IPSEΔNLS and IgE revealed a positively charged interaction interface which includes the IPSE/alpha-1-unique loop. Computational modeling suggested that the negatively charged region on the Cε2-domain of IgE provides a suitable binding interface for the positively charged IPSE/alpha-1 (**Fig. 11A+B**).

We therefore developed a model for the mechanism of basophil activation IPSE/alpha-1 (Fig. 11C), based on the computational modeling and our experimental data, specifically the inability of IPSE/alpha-1 to cross-link IgE, a putative 1:1 stoichiometry of IPSE/alpha-1-IgE complexes, and the binding of IPSE/alpha-1 to both, Fab and Fc fragments: The first monomer of the IPSE/alpha-1 dimer binds

the negatively charged surface of the C\$2 domain. Binding of the first IPSE/alpha-1 monomer to the IgE-Fc fragment facilitates binding of the second IPSE/alpha-1 monomer to the IgE-Fab. We hypothesize that this might trigger a conformational change of the IgE molecule in close proximity to the Fc\$-receptor and subsequent receptor activation without cross-linking. To validate this mechanism, further experiments are warranted to locate the binding site(s) of dimeric IPSE/alpha-1 on the IgE molecule by co-crystallization.

For the past 30 years, the receptor-mediated response to foreign antigens has been known to involve the high affinity IgE receptor on mast cells and basophils. Cross-linking of two or more IgE-receptor complexes on the cell surface stimulates degranulation of the cells and the release of mediators and cytokines (41). In contrast, IPSE/alpha-1 appeared to activate basophils by a novel mechanism that involves binding but not cross-linking receptor-bound IgE leaving the IgE "monomeric". A role of IgE monomers in initiating cell signaling upon binding to FceRI has been controversially discussed (42, 43). High concentrations of monomeric IgE were reported to partially activate the FceRI, thereby triggering cellular events such as degranulation and cytokine production (42). Moreover, different monoclonal IgEs seem to differ in their ability to activate basophils, but the structural differences that account for the functional divergence are not known (43). In contrast, Schweitzer-Stenner and Pecht consider non-physiological experimental conditions to cause the effects of monomeric IgE (44). Recently, however, the cross-linking model for cell activation has been challenged also for the T and B cell receptors (45, 46). It was shown that inactive T and B cell receptors are present in an oligomeric form, while binding of their respective ligands leads to dissociation into monomeric receptors and subsequent clustering of the monomeric receptors (dissociation model) (45, 47). Further studies are necessary to determine the mechanism of action IPSE/alpha-1. Since the solution methods used in this study do not necessarily reproduce the cell-surface environment in which IPSE/alpha-1 acts, further studies should reveal the structural rearrangement of FceRI-bound IgE on the cell surface upon binding of IPSE/alpha-1.

In conclusion, the parasite-derived protein IPSE/alpha-1 is the first member of the βγcrystallin superfamily discovered to have an immunomodulatory function. Additionally, this is the first report on the interaction of a crystallin-fold with IgE. Since in contrast to other known IgE-dependent basophil activators, IPSE/alpha-1 does not cross-link IgE, it appears to activate basophils via a novel mechanism. Our results regarding the structure and the molecular function of the basophil IL-4-inducing factor IPSE/alpha-1 help to better understand the mechanism by which parasites modulate the host's immune system and may provide a starting point for pharmacological intervention in the future.

Acknowledgements

The authors are grateful to Bernd Simon (EMBL Heidelberg), Gülden Demiraslan and Ulrike Schütz (Munich), Sven Mueller-Loennies and Niels Röckendorf (RCB, Borstel), and Prof. Brian J. Sutton and Prof. James M. McDonnell (King's College, London) for support and discussions. We thank the Bavarian NMR Centre (BNMRZ) for NMR time and the ESRF for access to measurements at beamline ID29. Editorial support was provided by David Young, Young Medical Communications and Consulting Ltd.

Conflict of Interest

The authors declare that they have no conflicts of interest with the contents of this article.

Author contributions

NHM, HH, MS and GS designed and coordinated this study and wrote the paper. NHM, KT, TM and MS designed, performed and analyzed NMR experiments, MH and JM-D solved the crystal structure, SiB performed and analyzed experiments shown in figure 4A and B, and figure 10A, B and D, DB provided technical assistance and performed experiments shown in figure 8, AM performed experiments shown in figure 5 and GS experiments shown in figure 4C and 10C. SB and AF designed and performed the peptide scan (figure 7D) and TK, TW and GS designed, performed and analyzed SPR assays (figure 6). All authors reviewed the results and approved the final version of the manuscript.

References

- 1. Schramm, G., and Haas, H. (2010) Th2 immune response against Schistosoma mansoni infection. *Microbes Infect*. **12**, 881–888
- 2. Seder, R. A., Paul, W. E., Davis, M. M., and Fazekas de St.Groth, B. (1992) The presence of interleukin 4 during in vitro priming determines the lymphokine-producing potential of CD4+ T cells from T cell receptor transgenic mice. *J.Exp.Med.* **176**, 1091–1098
- 3. Brunet, L. R., Finkelman, F. D., Cheever, A. W., Kopf, M. A., and Pearce, E. J. (1997) IL-4 protects against TNF-alpha-mediated cachexia and death during acute schistosomiasis. *J. Immunol.* **159**, 777–785
- 4. Herbert, D. R., Orekov, T., Perkins, C., Rothenberg, M. E., and Finkelman, F. D. (2008) IL-4R alpha expression by bone marrow-derived cells is necessary and sufficient for host protection against acute schistosomiasis. *J. Immunol.* **180**, 4948–4955
- 5. Sullivan, B. M., Liang, H. E., Bando, J. K., Wu, D., Cheng, L. E., McKerrow, J. K., Allen, C. D., and Locksley, R. M. (2011) Genetic analysis of basophil function in vivo. *Nat.Immunol.* **12**, 527–535
- 6. Van Panhuys, N., Prout, M., Forbes, E., Min, B., Paul, W. E., and Le Gros, G. (2011) Basophils are the major producers of IL-4 during primary helminth infection. *J. Immunol.* **186**, 2719–2728
- 7. Schramm, G., Falcone, F. H., Gronow, A., Haisch, K., Mamat, U., Doenhoff, M. J., Oliveira, G., Galle, J., Dahinden, C. A., and Haas, H. (2003) Molecular characterization of an interleukin-4-inducing factor from Schistosoma mansoni eggs. *J. Biol. Chem.* **278**, 18384–18392
- 8. Schramm, G., Mohrs, K., Wodrich, M., Doenhoff, M. J., Pearce, E. J., Haas, H., and Mohrs, M. (2007) Cutting edge: IPSE/alpha-1, a glycoprotein from Schistosoma mansoni eggs, induces IgE-dependent, antigen-independent IL-4 production by murine basophils in vivo. *J. Immunol.* **178**, 6023–6027
- 9. Schramm, G., Gronow, A., Knobloch, J., Wippersteg, V., Grevelding, C. G., Galle, J., Fuller, H., Stanley, R. G., Chiodini, P. L., Haas, H., and Doenhoff, M. J. (2006) IPSE/alpha-1: a major immunogenic component secreted from Schistosoma mansoni eggs. *Mol. Biochem. Parasitol.* **147**, 9–19
- 10. Dunne, D. W., Jones, F. M., and Doenhoff, M. J. (1991) The purification, characterization, serological activity and hepatotoxic properties of two cationic glycoproteins (alpha 1 and omega 1) from Schistosoma mansoni eggs. *Parasitology*. **103**, 225–236
- 11. Young, N. D., Jex, A. R., Li, B., Liu, S., Yang, L., Xiong, Z., Li, Y., Cantacessi, C., Hall, R. S., Xu, X., Chen, F., Wu, X., Zerlotini, A., Oliveira, G., Hofmann, A., Zhang, G., Fang, X., Kang, Y., Campbell, B. E., Loukas, A., Ranganathan, S., Rollinson, D., Rinaldi, G., Brindley, P. J., Yang, H., Wang, J., Wang, J., and Gasser, R. B. (2012) Whole-genome sequence of Schistosoma haematobium. *Nat. Genet.* 44, 221–225
- 12. Falcone, F. H., Dahinden, C. A., Gibbs, B. F., Noll, T., Amon, U., Hebestreit, H., Abrahamson, O., Klaucke, J., Schlaak, M., and Haas, H. (1996) Human basophils release interleukin-4 after stimulation with Schistosoma mansoni egg antigen. *Eur.J.Immunol.* **26**, 1147–1155
- 13. Watanabe, T., Inoue, T., Ochi, H., Terashima, M., Asano, Y., and Nakatani, T. (1999) Lipid A directly inhibits IL-4 production by murine Th2 cells but does not inhibit IFN-gamma production by Th1 cells. *Eur. J. Immunol.* **29**, 413–418

- 14. Patella, V., Florio, G., Petraroli, A., and Marone, G. (2000) HIV-1 gp120 induces IL-4 and IL-13 release from human FccRI+ cells through interaction with the VH3 region of IgE. *J.Immunol.* **164**, 589–595
- 15. Kaur, I., Schramm, G., Everts, B., Scholzen, T., Kindle, K. B., Beetz, C., Montiel-Duarte, C., Blindow, S., Jones, A. T., Haas, H., Stolnik, S., Heery, D. M., and Falcone, F. H. (2011) Interleukin-4-inducing principle from Schistosoma mansoni eggs contains a functional C-terminal nuclear localization signal necessary for nuclear translocation in mammalian cells but not for its uptake. *Infect.Immun.* **79**, 1779–1788
- 16. Wuhrer, M., Balog, C. I., Catalina, M. I., Jones, F. M., Schramm, G., Haas, H., Doenhoff, M. J., Dunne, D. W., Deelder, A. M., and Hokke, C. H. (2006) IPSE/alpha-1, a major secretory glycoprotein antigen from schistosome eggs, expresses the Lewis X motif on core-difucosylated N-glycans. *FEBS J.* 273, 2276–2292
- 17. Mayerhofer, H., Schramm, G., Hatzopoulos, G. N., Mueller-Dieckmann, C., Haas, H., and Mueller-Dieckmann, J. (2009) Cloning, expression, purification, crystallization and preliminary X-ray crystallographic analysis of interleukin-4-inducing principle from Schistosoma mansoni eggs (IPSE/alpha-1). *Acta Crystallogr.Sect.F.Struct.Biol.Cryst.Commun.* **65**, 594–596
- 18. Delaglio, F., Grzesiek, S., Vuister, G. W., Zhu, G., Pfeifer, J., and Bax, A. (1995) NMRPipe: a multidimensional spectral processing system based on UNIX pipes. *J.Biomol.NMR*. **6**, 277–293
- 19. Sattler, M., Schleucher, J., and Griesinger, C. (1999) Heteronuclear multidimensional NMR experiments for the structure determination of proteins in solution employing pulsed field gradients (1999) Prog. NMR Spectrosc. 34, 93-158. *Prog.NMR Spectrosc.* 34, 93-158
- 20. Meyer, N. H., Schramm, G., and Sattler, M. (2011) (1)H, (13)C and (15)N chemical shift assignments of IPSEDeltaNLS. *Biomol.NMR Assign*.
- 21. Farrow, N. A., Muhandiram, R., Singer, A. U., Pascal, S. M., Kay, C. M., Gish, G., Shoelson, S. E., Pawson, T., Forman-Kay, J. D., and Kay, L. E. (1994) Backbone dynamics of a free and phosphopeptide-complexed Src homology 2 domain studied by 15N NMR relaxation. *Biochemistry*. **33**, 5984–6003
- 22. Guntert, P. (2009) Automated structure determination from NMR spectra. *Eur. Biophys. J.* **38**, 129–143
- 23. Shen, Y., Delaglio, F., Cornilescu, G., and Bax, A. (2009) TALOS+: a hybrid method for predicting protein backbone torsion angles from NMR chemical shifts. *J.Biomol.NMR*. **44**, 213–223
- 24. Linge, J. P., Williams, M. A., Spronk, C. A., Bonvin, A. M., and Nilges, M. (2003) Refinement of protein structures in explicit solvent. *Proteins*. **50**, 496–506
- 25. Nederveen, A. J., Doreleijers, J. F., Vranken, W., Miller, Z., Spronk, C. A., Nabuurs, S. B., Guntert, P., Livny, M., Markley, J. L., Nilges, M., Ulrich, E. L., Kaptein, R., and Bonvin, A. M. (2005) RECOORD: a recalculated coordinate database of 500+ proteins from the PDB using restraints from the BioMagResBank. *Proteins.* **59**, 662–672
- 26. Laskowski, R. A., Rullmannn, J. A., MacArthur, M. W., Kaptein, R., and Thornton, J. M. (1996) AQUA and PROCHECK-NMR: programs for checking the quality of protein structures solved by NMR. *J.Biomol.NMR*. **8**, 477–486
- 27. Hooft, R. W., Vriend, G., Sander, C., and Abola, E. E. (1996) Errors in protein structures. *Nature*. **381**, 272
- 28. Riek, R., Wider, G., Pervushin, K., and Wuthrich, K. (1999) Polarization transfer by cross-correlated relaxation in solution NMR with very large molecules. *Proc.Natl.Acad.Sci.U.S.A.* **96**, 4918–4923

- 29. Otwinowski, Z., and Minor, W. (1997) [20] Processing of X-ray diffraction data collected in oscillation mode. in *Methods in Enzymology* (Charles W. Carter, J. ed), pp. 307–326, Macromolecular Crystallography Part A, Academic Press, **Volume 276**, 307–326
- 30. McCoy, A. J., Grosse-Kunstleve, R. W., Adams, P. D., Winn, M. D., Storoni, L. C., and Read, R. J. (2007) Phaser crystallographic software. *J Appl Crystallogr.* **40**, 658–674
- 31. Murshudov, G. N., Skubák, P., Lebedev, A. A., Pannu, N. S., Steiner, R. A., Nicholls, R. A., Winn, M. D., Long, F., and Vagin, A. A. (2011) REFMAC5 for the refinement of macromolecular crystal structures. *Acta Crystallogr. D Biol. Crystallogr.* **67**, 355–367
- 32. Emsley, P., Lohkamp, B., Scott, W. G., and Cowtan, K. (2010) Features and development of Coot. *Acta Crystallogr. D Biol. Crystallogr.* **66**, 486–501
- 33. Chen, V. B., Arendall, W. B., Headd, J. J., Keedy, D. A., Immormino, R. M., Kapral, G. J., Murray, L. W., Richardson, J. S., and Richardson, D. C. (2010) MolProbity: all-atom structure validation for macromolecular crystallography. *Acta Crystallogr. D. Biol. Crystallogr.* **66**, 12–21
- 34. Comeau, S. R., Gatchell, D. W., Vajda, S., and Camacho, C. J. (2004) ClusPro: a fully automated algorithm for protein-protein docking. *Nucleic Acids Res.* **32**, W96–99
- 35. Roeckendorf, N., Bade, S., Hirst, T. R., Gorris, H. H., and Frey, A. (2007) Synthesis of a fluorescent ganglioside GM1 derivative and screening of a synthetic peptide library for GM1 binding sequence motifs. *Bioconjug.Chem.* **18**, 573–578
- 36. Haisch, K., Gibbs, B. F., K"rber, H., Ernst, M., Grage-Griebenow, E., Schlaak, M., and Haas, H. (1999) Purification of morphologically and functionally intact human basophils to near homogeneity. *J.Immunol.Methods.* **226**, 129–137
- 37. Mathieson, W., and Wilson, R. A. (2010) A comparative proteomic study of the undeveloped and developed Schistosoma mansoni egg and its contents: The miracidium, hatch fluid and secretions. *Int.J.Parasitol.* **40**, 617–628
- 38. Jaenicke, R., and Slingsby, C. (2001) Lens crystallins and their microbial homologs: structure, stability, and function. *Crit Rev. Biochem. Mol. Biol.* **36**, 435–499
- 39. Hemmingsen, J. M., Gernert, K. M., Richardson, J. S., and Richardson, D. C. (1994) The tyrosine corner: a feature of most Greek key beta-barrel proteins. *Protein Sci.* **3**, 1927–1937
- 40. Smith, P., Fallon, R. E., Mangan, N. E., Walsh, C. M., Saraiva, M., Sayers, J. R., McKenzie, A. N. J., Alcami, A., and Fallon, P. G. (2005) Schistosoma mansoni secretes a chemokine binding protein with antiinflammatory activity. *J. Exp. Med.* **202**, 1319–1325
- 41. Holowka, D., Sil, D., Torigoe, C., and Baird, B. (2007) Insights into immunoglobulin E receptor signaling from structurally defined ligands. *Immunol.Rev.* **217**, 269–279
- 42. Kitaura, J., Xiao, W., Maeda-Yamamoto, M., Kawakami, Y., Lowell, C. A., and Kawakami, T. (2004) Early divergence of Fc epsilon receptor I signals for receptor upregulation and internalization from degranulation, cytokine production, and survival. *J.Immunol.* **173**, 4317–4323
- 43. Kitaura, J., Song, J., Tsai, M., Asai, K., Maeda-Yamamoto, M., Mocsai, A., Kawakami, Y., Liu, F. T., Lowell, C. A., Barisas, B. G., Galli, S. J., and Kawakami, T. (2003) Evidence that IgE molecules mediate a spectrum of effects on mast cell survival and activation via aggregation of the FcepsilonRI. *Proc.Natl.Acad.Sci.U.S.A.* **100**, 12911–12916
- 44. Schweitzer-Stenner, R., and Pecht, I. (2005) Death of a dogma or enforcing the artificial: monomeric IgE binding may initiate mast cell response by inducing its receptor aggregation. *J.Immunol.* **174**, 4461–4464

- 45. Yang, J., and Reth, M. (2010) Oligomeric organization of the B-cell antigen receptor on resting cells. *Nature*. **467**, 465–469
- 46. Lillemeier, B. F., Mortelmaier, M. A., Forstner, M. B., Huppa, J. B., Groves, J. T., and Davis, M. M. (2010) TCR and Lat are expressed on separate protein islands on T cell membranes and concatenate during activation. *Nat.Immunol.* 11, 90–96
- 47. Yang, J., and Reth, M. (2010) The dissociation activation model of B cell antigen receptor triggering. *FEBS Lett.* **584**, 4872–4877
- 48. Baker, N. A., Sept, D., Joseph, S., Holst, M. J., and McCammon, J. A. (2001) Electrostatics of nanosystems: application to microtubules and the ribosome. *Proc.Natl.Acad.Sci.U.S.A.* **98**, 10037–10041

Footnotes

K.T. acknowledges support by the Alexander von Humboldt foundation; T.M. by an EMBO Long Term Fellowship, a Schrödinger Fellowship by the Austrian Science Fund (FWF) and an APART-fellowship (Austrian Academy of Sciences). This work was supported by the Deutsche Forschungsgemeinschaft (EXC114 and SFB 594) (M.S) and the Bavarian Ministry of Sciences, Research and the Arts in the framework of the Bavarian Molecular Biosystems Research Network (T.M.).

Figure Legends

- FIGURE 1. **Biochemical and NMR analysis of Proteins studied**. (A) Schematic depiction of different mutants of IPSE/alpha-1. The monomeric IPSEΔNLS was used for structural analysis. (B) Comparison of recombinantly expressed and purified IPSE wt and IPSEΔNLS by SDS-PAGE and silver staining under non-reducing (non-red) and reducing (red) conditions. (C) Primary sequence, secondary structure, NMR ¹³C secondary chemical shifts and (D) { ¹H}-¹⁵N heteronuclear NOE of IPSEΔNLS.
- FIGURE 2. Structure of IPSEΔNLS. (A) NMR (left) and crystal (right) structure of IPSEΔNLS. (B) Secondary structure topology of IPSEΔNLS. (C) Ribbon representation of the NMR-derived structure of IPSEΔNLS. Cysteine residues involved in disulfide bridges and the unique loop of the IPSE crystallin fold are indicated. (D) Zoomed view highlighting amino acids of the Greek key signature sequence (red sticks).
- FIGURE 3. **IPSEΔNLS** adopts a βγ-crystallin fold. (A) Zoomed view of IPSEΔNLS (blue, right) and human eye lens γ -B-crystallin (dark yellow, left). Shown are the residues of the tyrosine-corner of γ -B-crystallin (Tyr151 and Arg147) and the orthogonal stacked Tyr72 and 74 as well as the disulfide bridges of IPSEΔNLS (sticks) and the flexible loop (aa 62-69) (green). (B) Structure superposition of two IPSEΔNLS monomers (blue) with dimeric Spherulin 3A (orange). Structures align with a backbone RMSD of 1.8 Å. (C) Structure-based multiple sequence alignment of crystallin superfamily members. Above the sequences: secondary structure elements of IPSEΔNLS (except of disulfide bridges). Below the sequences: disulfide bridges are shown as red numbers; the flexible loop (aa 62-69) unique to IPSE/alpha-1 is depicted as a green bar; the two F/YXXXXF/YG signature sequences and the conserved serine residues characteristic of the crystallin fold are indicated by asterisks.
- FIGURE 4. IPSE/alpha-1 is an immunoglobulin-binding protein with highest affinity to IgE. (A) IPSE/alpha-1 binds to immunoglobulins and transferrin (Tf) in human serum. Western Blots of human serum were incubated with IPSE/alpha-1 followed by labeled streptavidin (SAV-AP) or labeled α -human IgG. Proteins were stained with AuroDye and India Ink. (B) IPSE/alpha-1 binds to various immunoglobulin isotypes. Strips with blotted human polyclonal IgE, IgG, IgA and IgM were incubated with the respective anti-isotype antibodies or IPSE/alpha-1 followed by SAV-AP. Controls: Secondary antibody (C1), SAV-AP (C2). (C) Dotted IgG and IgE were incubated with labeled IPSE/alpha-1 followed by SAV-AP.
- FIGURE 5. **Size Exclusion Chromatography**. (A) Complexes of IPSE/alpha-1 and IgE and (B) complexes of IPSE/alpha-1 and IgG (ratio 1:1), respectively, were applied to a Superdex 75 column (red curve). For control the same amount IPSE/alpha-1 alone (green curve) and IgE or IgG alone (blue curve) were run over the column. Fractions of the IPSE/alpha-1-IgE or -IgG complexes were analyzed by SDS-PAGE and silver staining. High molecular weight fractions contain IPSE/alpha-1 and IgE but not IgG, suggesting that IPSE/alpha-1 binds with higher affinity to IgE than to IgG.
- FIGURE 6. Surface Plasmon Resonance assays. Binding of IPSE/alpha-1 dimer (A) and IPSE Δ NLS monomer (B) to IgE and IgG immobilized on a CM5 chip was analysed by real-time measurement. Curves were obtained after subtraction of the unspecific binding to the reference cell. Bound IPSE (RU) was estimated at the end of the association phase. Binding isotherms of the IPSE/alpha-1 dimer (A) showed a sigmoidal curve characteristic for multivalent positive cooperative binding. Thus, Langmuir (1:1) calculation of affinity constants was not applicable. For the IPSE Δ NLS monomer (B) dissociation constants of 1.7 μ M and 7.4 μ M for IgE and IgG, respectively, were measured.
- FIGURE 7. Mapping the binding surface of IPSEANLS with IgE. (A) 1 H, 15 N NMR correlation spectra of IPSEANLS (black) and the IPSEANLS/IgE complex (molecular weight ~ 200 kDa, red). The presence of NMR signals corresponding to free IPSEANLS at a molar ratio of ~1:1 (IPSEANLS: IgE) suggests that IgE has only one IPSEANLS binding site. (Note, the NMR signals of even a very small fraction of free IPSEANLS (10 kDa) are much stronger than those of the 200 kDa complex). (B)

NMR chemical shift perturbation (CSP) vs. residue number. Blue negative bars indicate amide signals that are broadened beyond detection. (C) Mapping of the IgE binding interface onto the structure of IPSE Δ NLS. Nitrogen atoms of the backbone amide groups are represented as spheres and colored red according to CSP or blue if line broadening is observed in the NMR titration experiment. (D) Peptide Scan: Binding of labeled IgE to immobilized 15-mer IPSE-derived peptides. Binding (mean \pm standard error of the mean) of IgE-DY781 to 15mer peptides is expressed in relation to the IPSE-derived peptide 62 - 76 (inset: spots D1 and D2; mean fluorescence = 100%). Residues exchanged to Ala or Glu in the respective peptides are highlighted in red. Inset: representative example of a peptide library read-out.

FIGURE 8. Mutational analysis of immunoglobulin binding and functional activity of IPSE/alpha-1. (A) Binding of IPSE/alpha-1 wild-type and protein mutants to monoclonal anti-IPSE antibody, human IgG and human IgE, analyzed by Western blots. Mutants in red boxes were analyzed by SPR for binding affinity with IgE. (B) IL-4 release from human basophils induced by different concentrations of IPSE/alpha-1 wild-type and mutants, respectively. Shown is one representative result of three independent experiments. (C) Surface representation of IPSEΔNLS: Binding interface, derived from the NMR titration and the peptide scan (orange).

FIGURE 9. 1D ¹H NMR (A) and ¹H, ¹⁵N HSQC spectra (B) spectra of IPSEΔNLS and IPSEΔNLS mutants. (A) Spectral regions of amide, aromatic and methyl protons for the mutants Q28R/E41K, K67E/R68E, F62A/N64A, I108E/K109E and D31K/E32K are shown. The good dispersion of amide proton signals and the presence of methyl proton signals below 0 ppm observed for all variants except I108E/K109 are indicative of the presence of tertiary folds. Signals arising from low molecular weight contaminations are marked with an asterisk. Spectra were recorded at 600 MHz ¹H Larmor frequency. (B) Only signals of amides in close spatial proximity to the mutations are shifted in the spectra of D31K/E32K and K67E/R68E mutants. Spectra were recorded at 600 MHz ¹H Larmor frequency.

FIGURE 10. Mode of interaction of IPSE/alpha-1 with immunoglobulins. (A) Binding of IPSE/alpha-1 to deglycosylated IgG Fc. Blotted mock-treated IgG Fc (Control) and IgG Fc deglycosylated with PNGase F were incubated with α-human IgG Fc or Aleuria aurantia agglutinin (AAA) or labeled IPSE/alpha-1. (B) IPSE/alpha-1 binds to Fab and Fc fragments. Blotted Fab and Fc fragments of human IgG were detected by α -human IgG (Fc), by α -kappa light chain (α -Ig kappa), by AAA or by labeled IPSE/alpha-1. C1 = buffer control, C2 = SAV-AP. (C) Sandwich-blots. Human IgE dotted at different amounts (10 - 0.1 pmol) was incubated with buffer (negative control) or α -IgE (positive control) or IPSE/alpha-1, followed by biotinylated IgE. α-IgE gives a clear signal with a maximum at 0.3 pmol / dot, while IPSE/alpha-1 does not exceed background level. (D) Double immunodiffusion assay (Ouchterlony). Binding partners were applied at various ratios. One partner was pipetted into the centre well, the other one clockwise beginning at 12 o'clock in order of dilution in the surrounding wells: 1:1, 1:2, 1:4, 1.8, 1:16, and 1:32. The following starting concentrations were used: 0.5 mg/ml IgE and 1 mg/ml anti-IgE; 0.5 mg/ml IgG and 0.5 mg/ml anti-IgG; 0.5 mg/ml IgG and 0.5 mg/ml protein L (a B cell superantigen from Peptostreptococcus magnus); 0.25 mg/ml IgE and 0.05 mg/ml IPSE/alpha-1 (corresponds to a molar ratio of approximately 1:1); 0.25 mg/ml IgG and 0.05 mg/ml IPSE/alpha-1 and 0.05 mg/ml IPSE/alpha-1 and rabbit anti-IPSE antiserum (1:2). Precipitation arcs indicate complex formation.

FIGURE 11. Model of the interaction of IPSE/alpha-1 with IgE: A putative novel mechanism of basophil activation. (A) Surface representation of IgE Fc (PDB accession code 2Y7Q, left) and IPSE Δ NLS (right) colored according to electrostatic surface potential at ± 2 kB T/e for positive (blue) or negative (red) charge potential using the program APBS (48). (B) Proposed interaction between IPSE Δ NLS and IgE (represented by the crystal structure of IgE Fc/Fc ϵ RI, PDB accession code 2WQR). The positively charged binding interface of IPSE Δ NLS mapped by NMR and mutational analysis presumably interacts with a negatively charged surface on the, while the Fc ϵ RI binds to the neighboring C ϵ 3 domain of the IgE molecule. (C) Schematic model of IgE receptor activation on the

surface of basophils. IPSE/alpha-1 may induce a structural rearrangement in the IgE molecule. This triggers the activation of the receptor signaling cascade.

Table 1: Refinement statistics for IPSE∆NLS

A) NMR Solution structure

	IPSEΔNLS
Distance constraints	•
Total NOE	2650
Intra-residue	651
Inter-residue	
Sequential $(i-j =1)$	499
Medium-range $(i-j < 4)$	286
Long-range $(i-j > 5)$	1214
Intermolecular	0
Hydrogen bonds	0
Total dihedral angle restraints	161
φ	80
Ψ	81
Structure statistics	
Violations (mean and s.d.)	
Distance constraints (Å)	0.009 ± 0.001
Dihedral angle constraints (°)	0.908 ± 0.053
Max. dihedral angle violation (°)	6.05
Max. distance constraint violation (Å)	0.18
Deviations from idealized geometry	
Bond lengths (Å)	0.016
Bond angles (°)	1.307
Impropers (°)	1.248
Average pairwise r.m.s. deviation** (Å)	
Heavy	0.77 ± 0.06
Backbone	0.32 ± 0.05

Pairwise r.m.s. deviation was calculated among 20 refined structures for residues 25-121

B) Crystal structure

	IPSEΔNLS
Refinement	
Resolution (Å)	47.1-1.71
No. reflections	10323
$R_{ m work}$ / $R_{ m free}$	15.4 / 17.7
No. atoms	
Protein	798
Water	122
B-factors	
Protein	17.1
Water	27.3
R.m.s. deviations	
Bond lengths (Å)	0.011
Bond angles (°)	1.36

C) X-ray data-collection and processing statistics

X-ray source	ID29, ESRF
Wavelength (Å)	0.9762
Space group	P61
Unit-cell parameters (Å,°)	$a = b = 54.40, c = 56.71, \gamma = 120$
Observed reflections	83352
Resolution	47.11 - 1.71 (1.768 - 1.71)
Completeness %)	99.03 (92.07)
$I/\sigma(I)$	22.8 (3.66)
Multiplicity	7.4 (4.0)

Figure 1

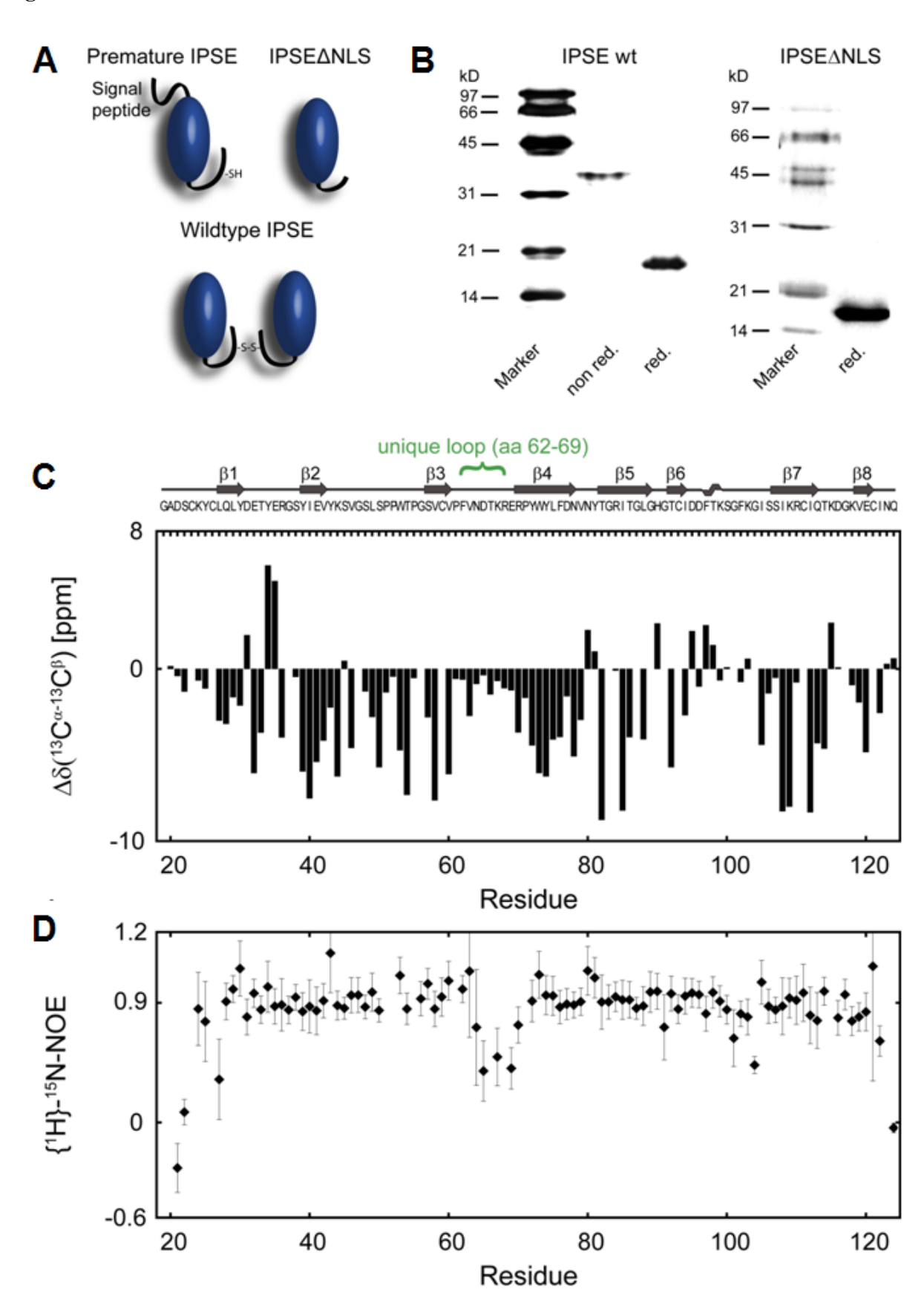
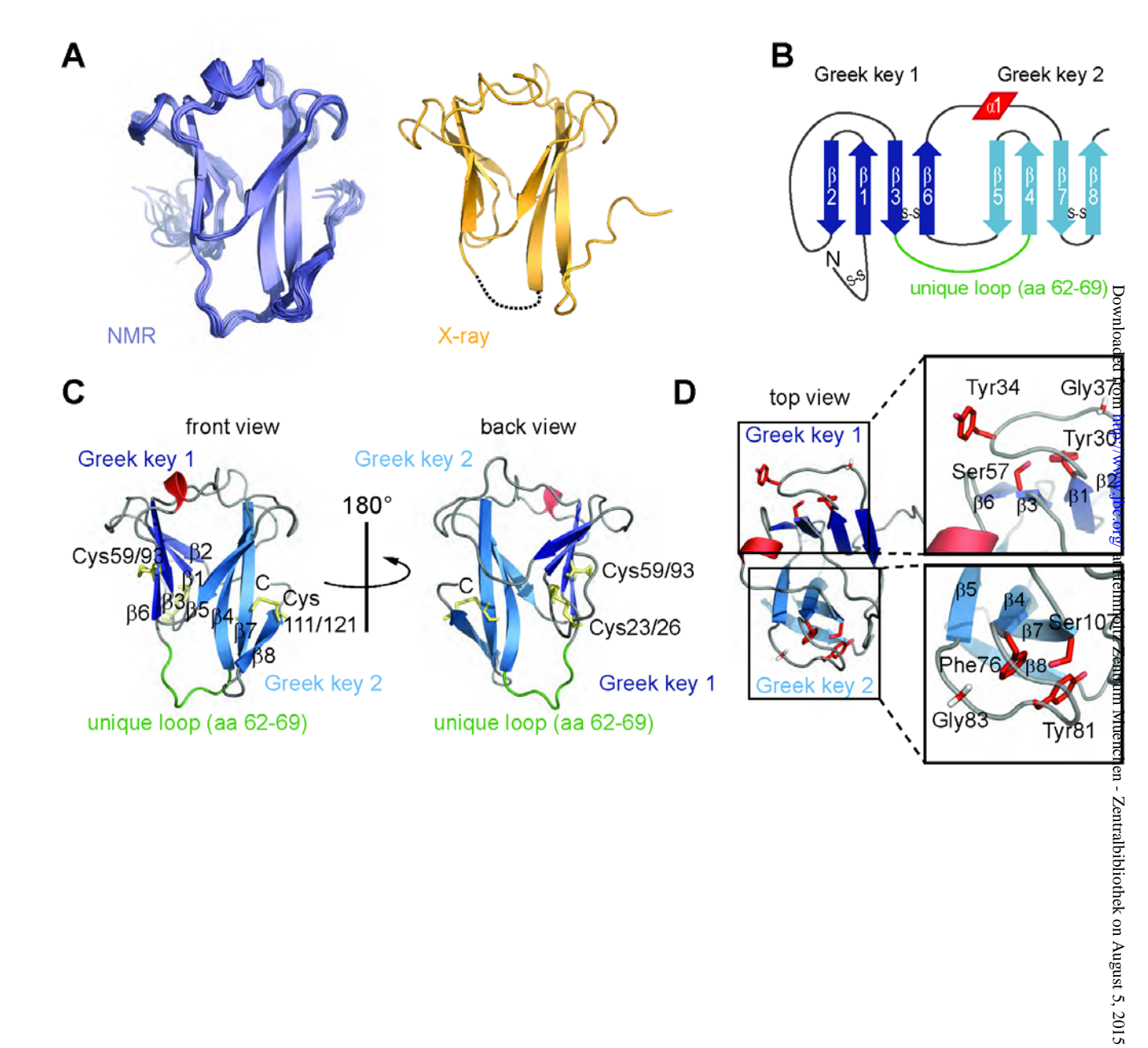


Figure 2



22

Figure 3

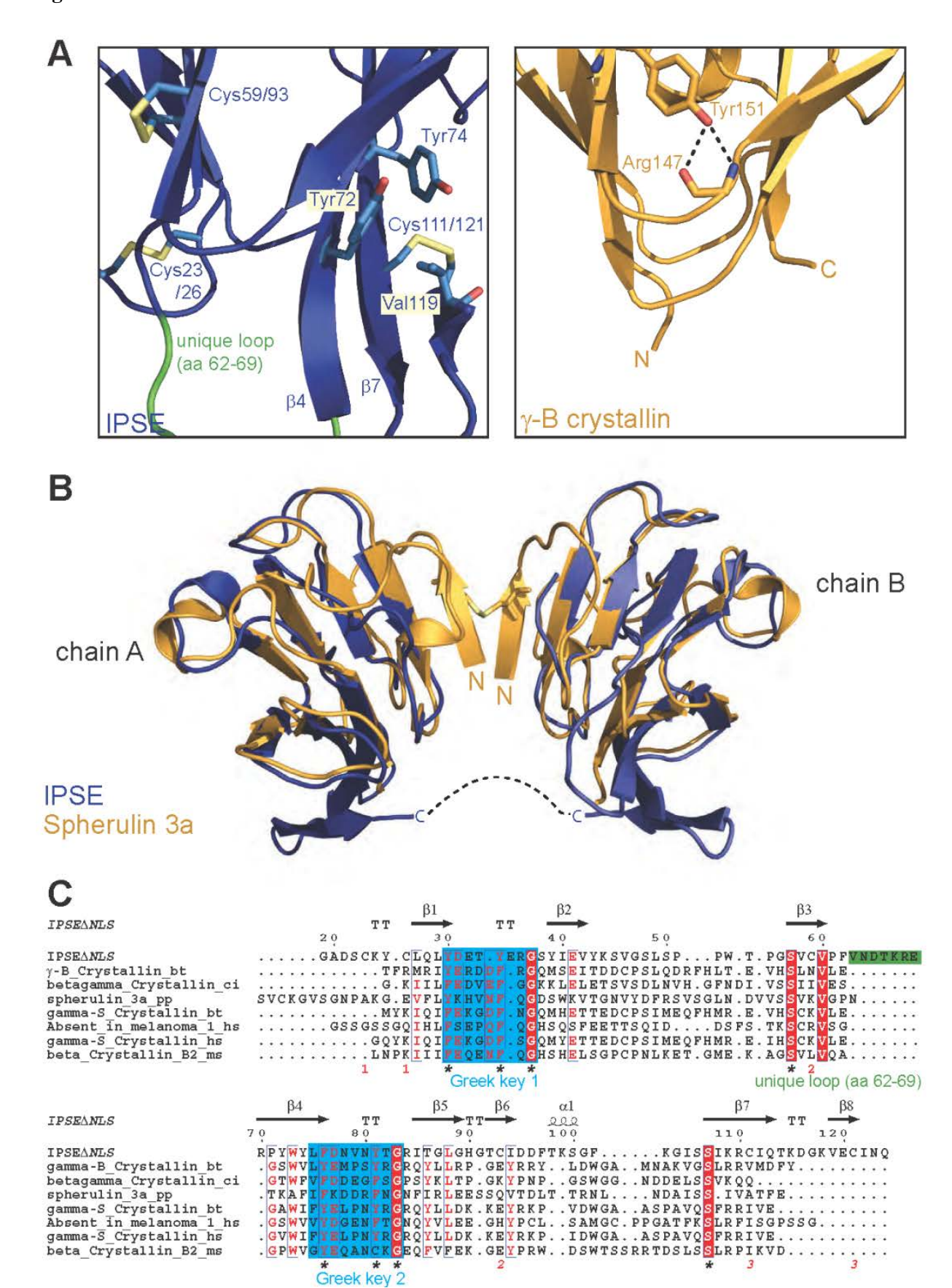


Figure 4

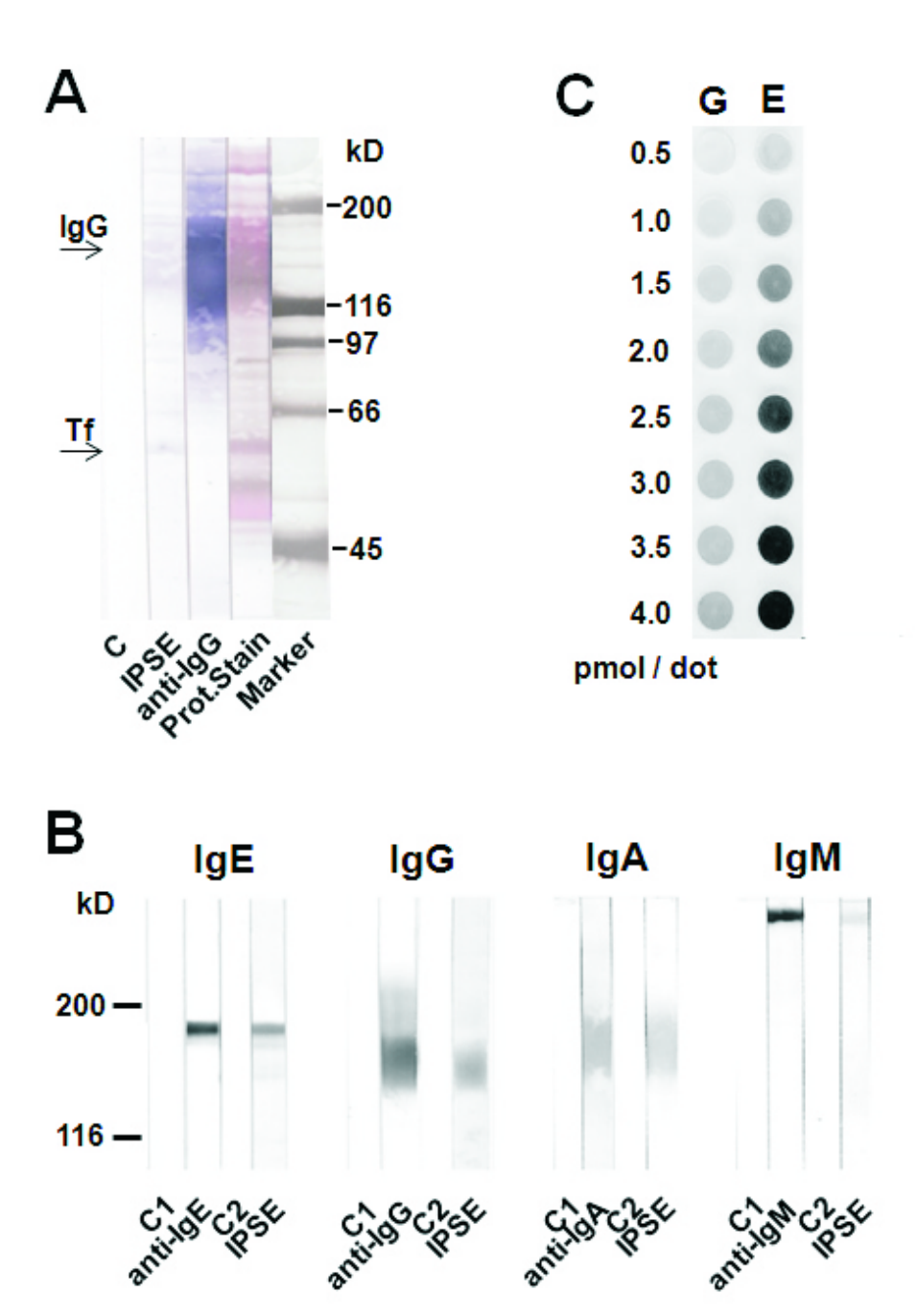
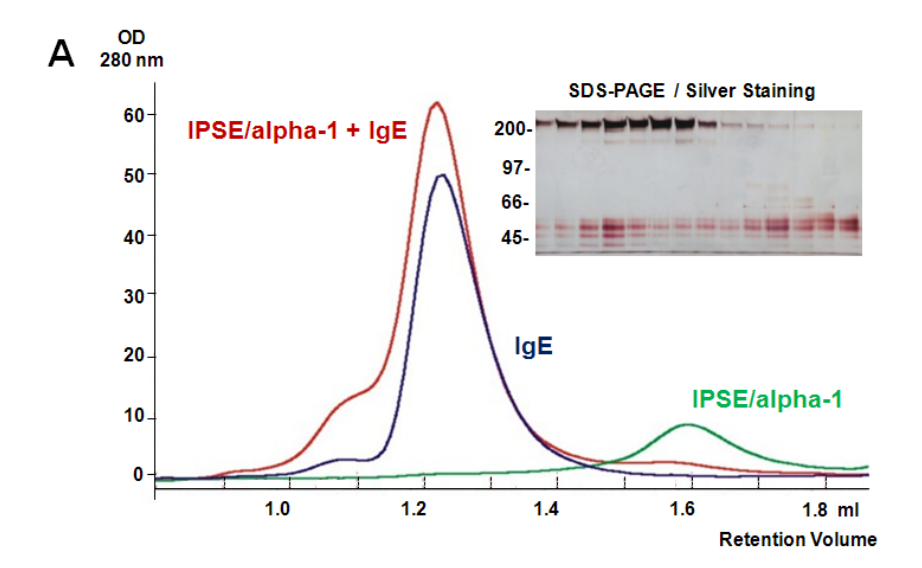


Figure 5



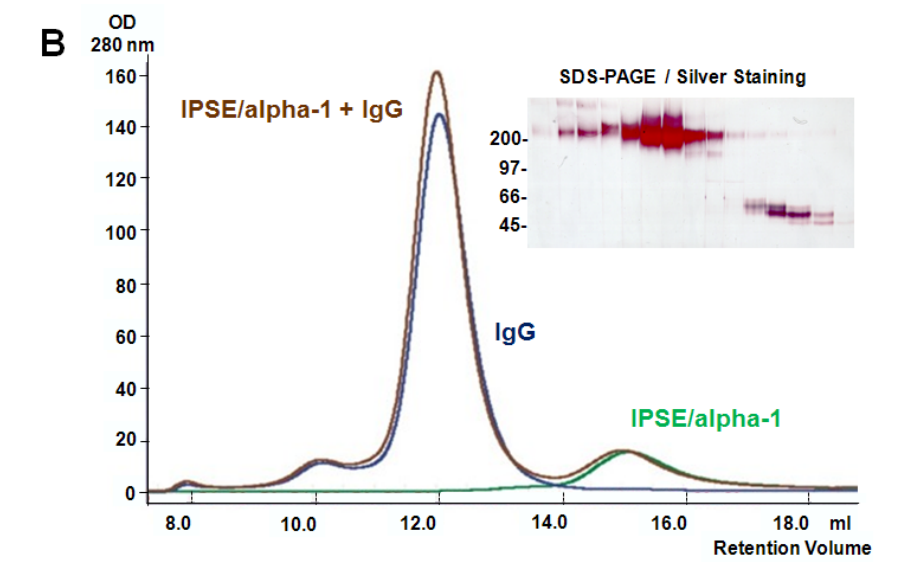


Figure 6

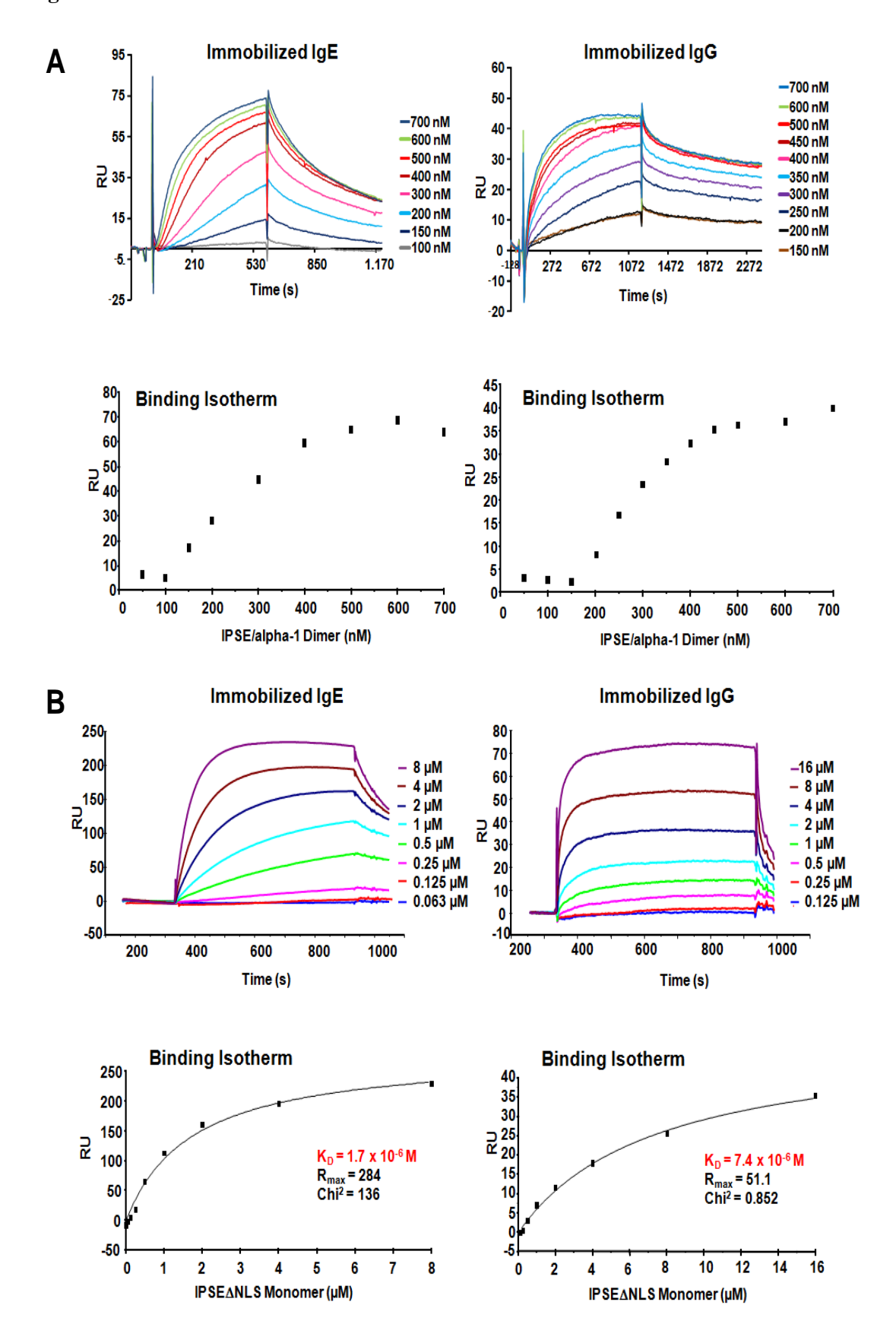


Figure 7

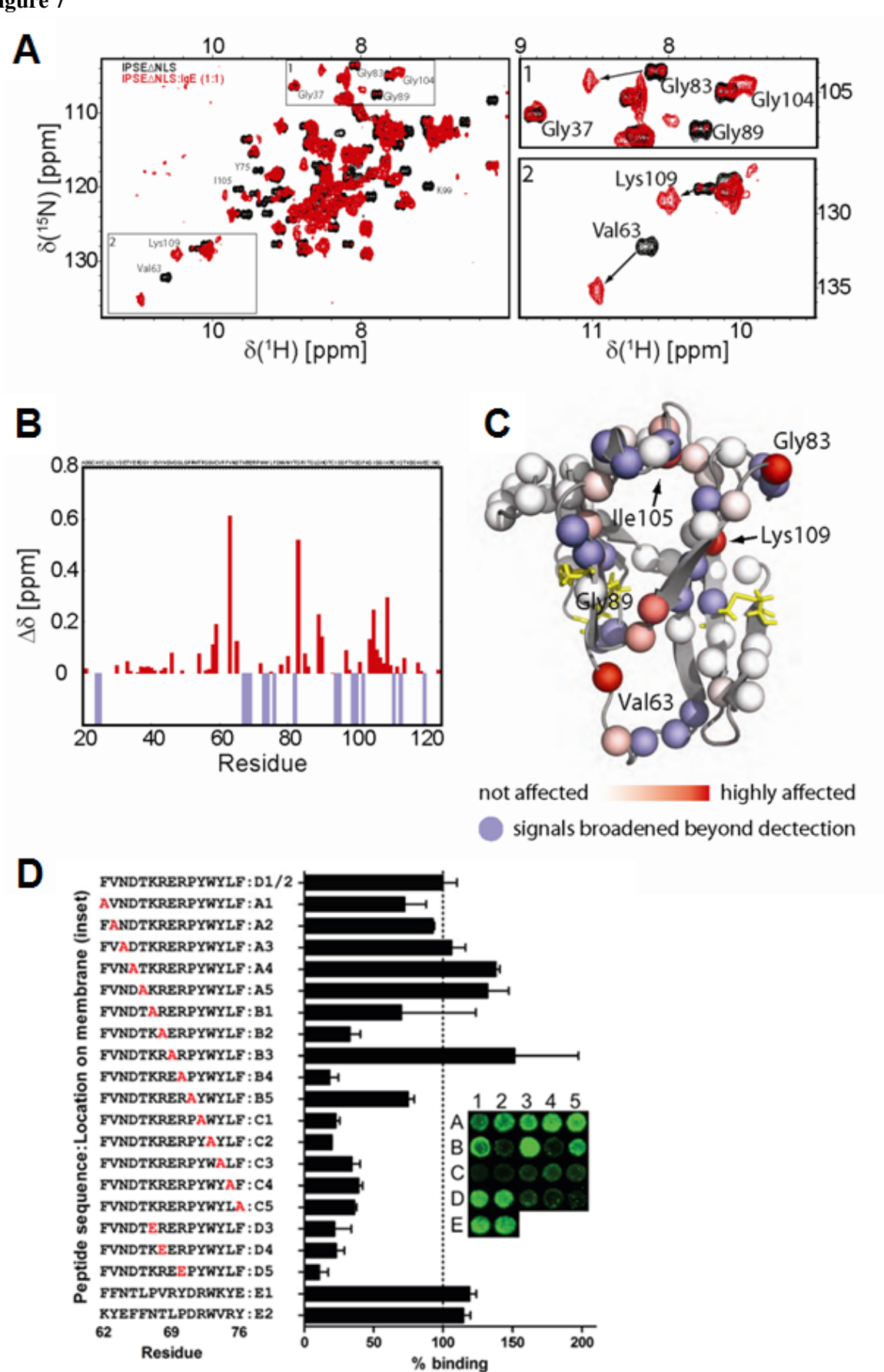
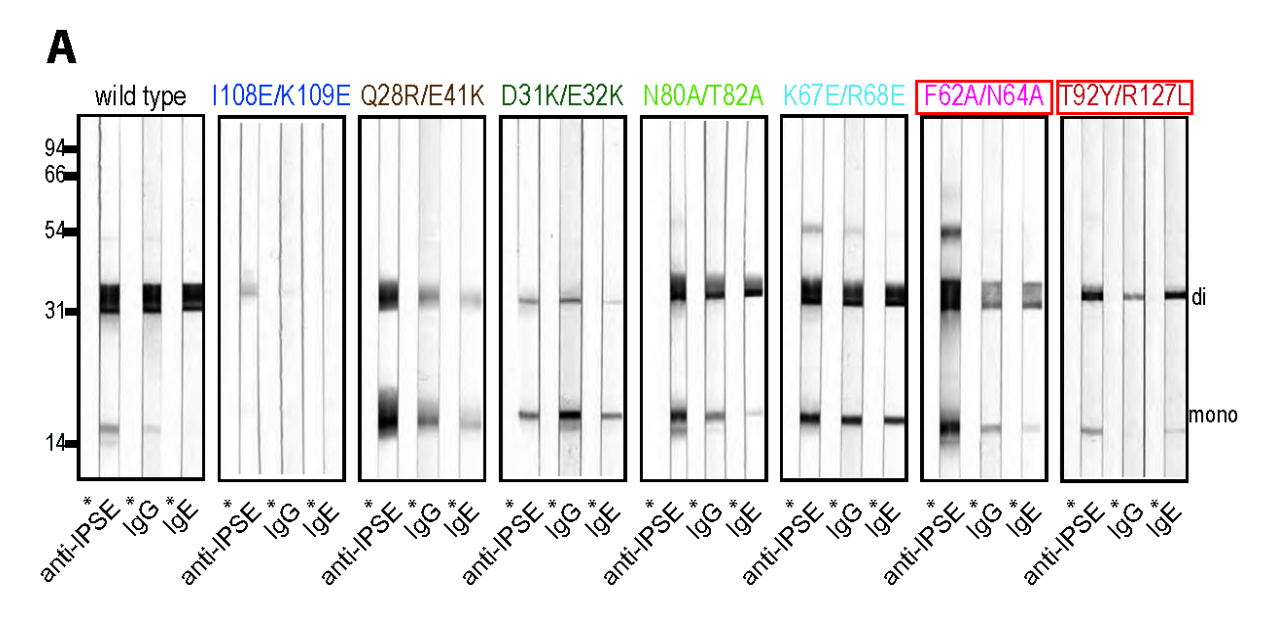
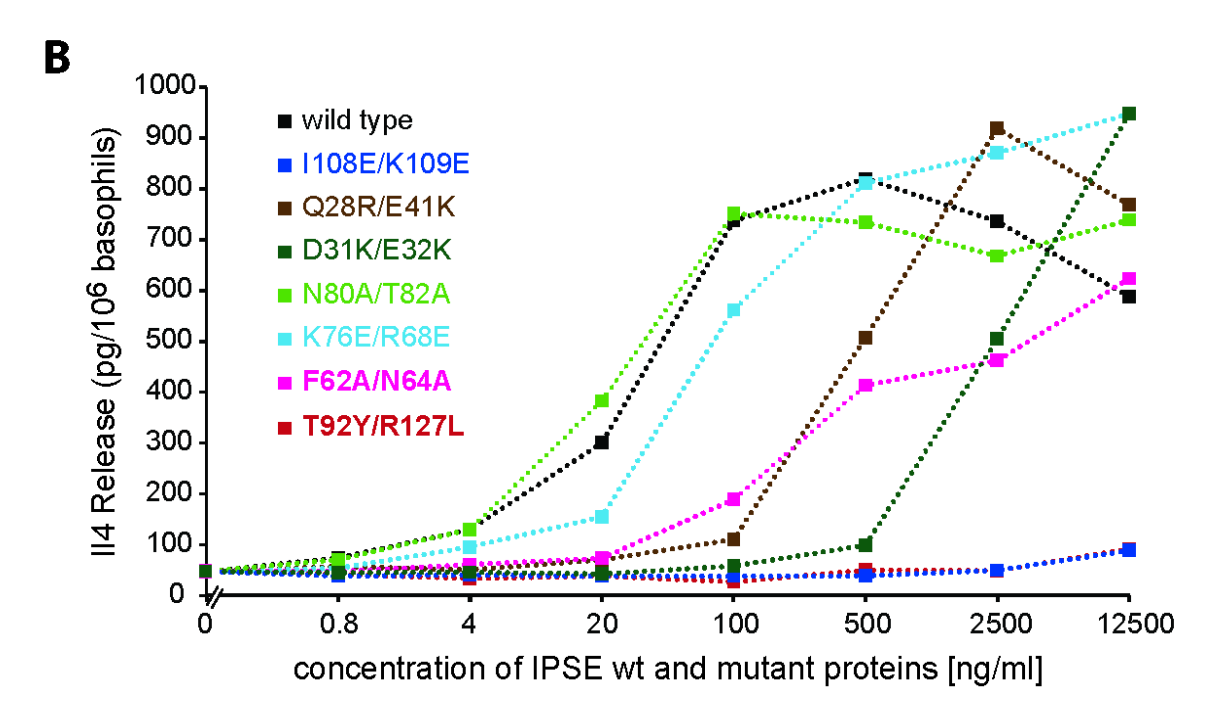


Figure 8





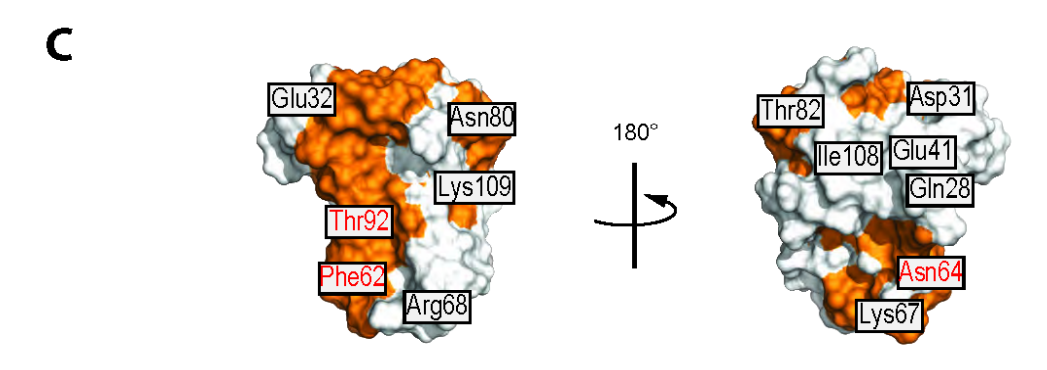


Figure 9

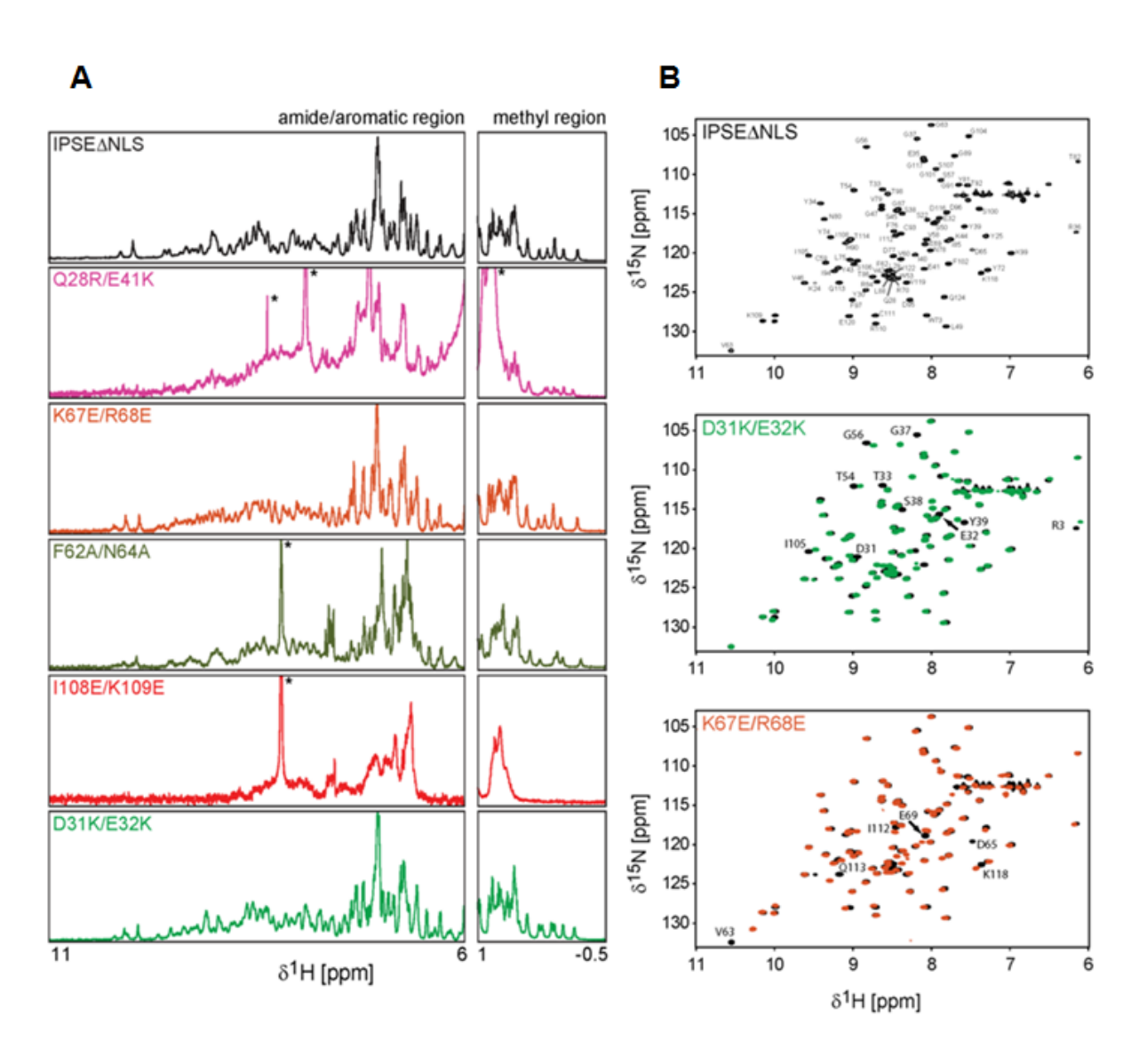


Figure 10

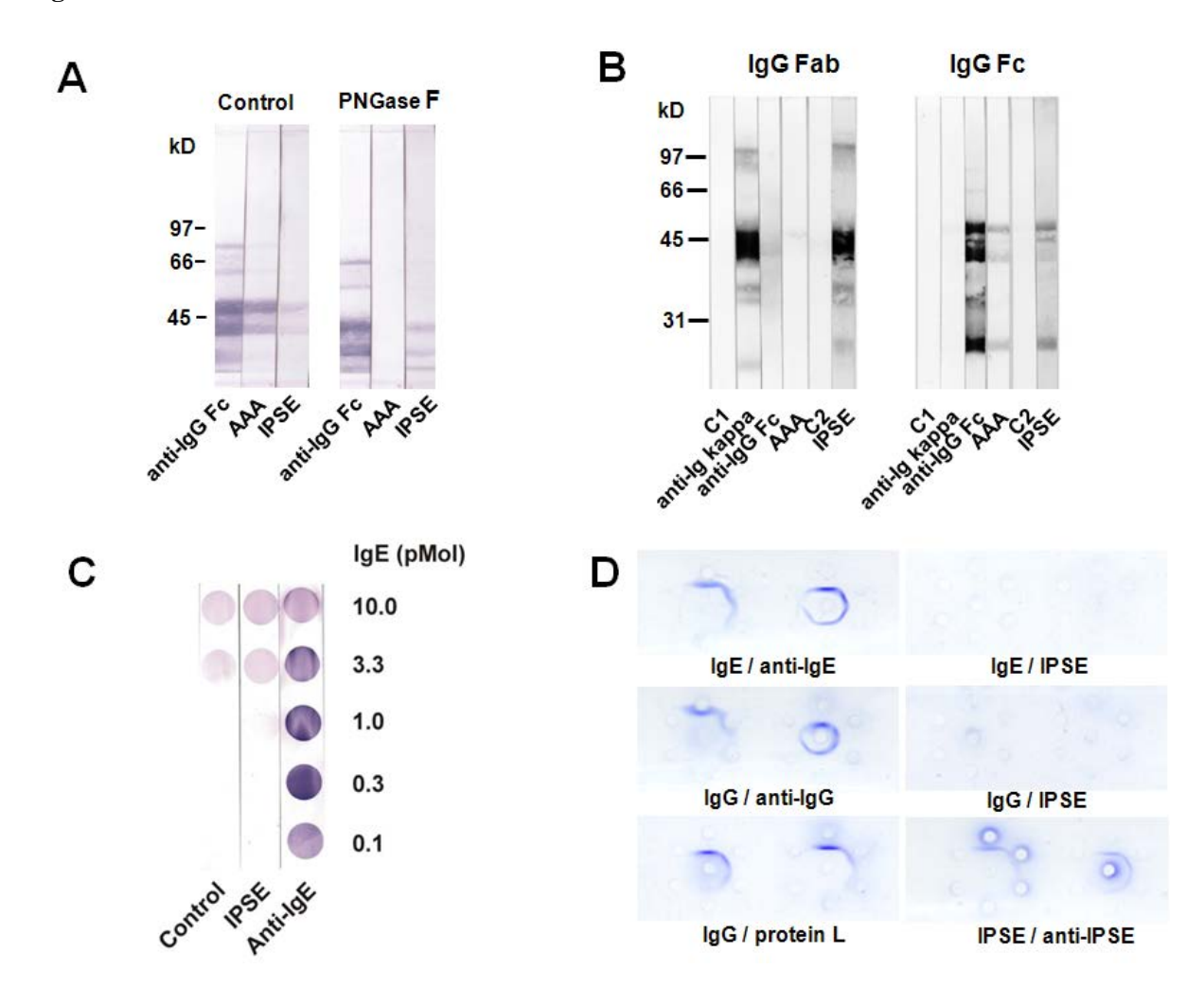
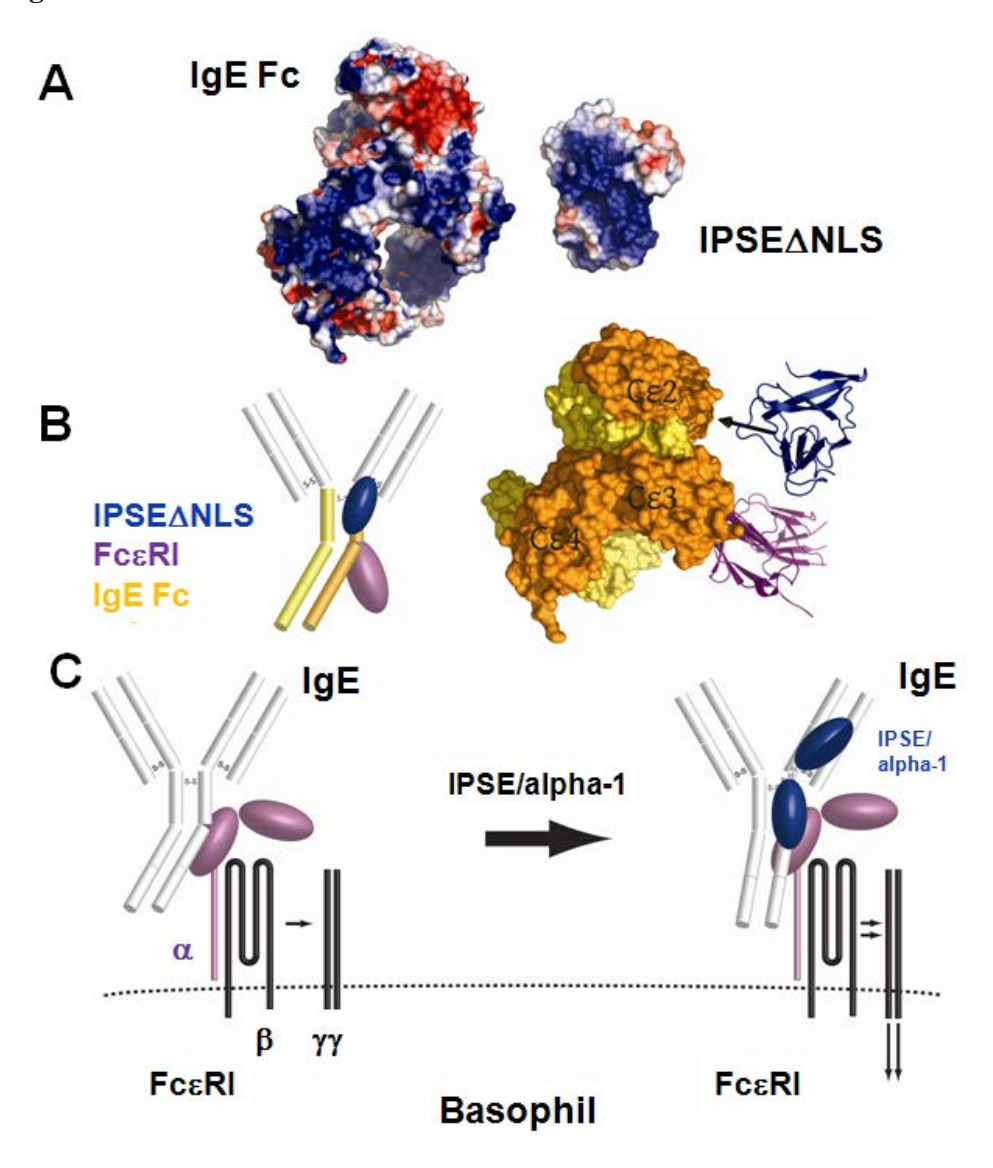


Figure 11





Immunology:

A crystallin fold in the interleukin-4-inducing principle of Schistosoma mansoni eggs (IPSE/alpha-1) mediates IgE binding for antigen-independent basophil activation





Access the most updated version of this article at doi: 10.1074/jbc.M115.675066

Find articles, minireviews, Reflections and Classics on similar topics on the JBC Affinity Sites.

Alerts:

- · When this article is cited
- When a correction for this article is posted

Click here to choose from all of JBC's e-mail alerts

This article cites 0 references, 0 of which can be accessed free at http://www.jbc.org/content/early/2015/07/10/jbc.M115.675066.full.html#ref-list-1